Industrial Crops & Products 226 (2025) 120753

Contents lists available at ScienceDirect

Industrial Crops & Products

journal homepage: www.elsevier.com/locate/indcrop

Spatiotemporal trends of rubber defoliation and refoliation and their responses to abiotic factors in the northern edge of the Asian tropics

Yanling Chen [a,b], Nuttapon Khongdee [c], Yaofeng Wang [d], Qinghai Song [e], Dengsheng Lu [a,b], Shusen Wang [f], Yaoliang Chen [a,b,*]

[a] Key Laboratory of Humid Subtropical Eco-Geographical Process of Ministry of Education, Fujian Normal University, Fuzhou 350117, China
[b] School of Geographical Sciences, Fujian Normal University, Fuzhou 350117, China
[c] Department of Highland Agriculture and Natural Resources, Faculty of Agriculture, Chiang Mai University, Chiang Mai 50200, Thailand
[d] Zhoushan Natural Resources Surveying and Mapping Design Center, Zhoushan 316000, China
[e] CAS Key Laboratory of Tropical Forest Ecology, Xishuangbanna Tropical Botanical Garden, Chinese Academy of Sciences, Menglun 666303, China
[f] Canada Centre for Remote Sensing, Natural Resources Canada, Ottawa K1A 0E4, Canada

ARTICLE INFO

Key words:
Phenology
Rubber plantation
Vegetation index
Spatiotemporal pattern
Abiotic factors

ABSTRACT

Hevea brasiliensis, a species native to evergreen broadleaf forest in Amazon tropical regions, exhibits a concentrated period of defoliation and refoliation after introduced to the northern edge of Asian tropics. However, up to date, spatiotemporal patterns of rubber phenology and the underlying mechanism remain unclear. In this study, we first investigated the optimal vegetation indices in monitoring four key rubber phenology metrics (i.e., Start of Defoliation (SOD), End of Defoliation (EOD), Start of Refoliation (SOR), and End of Refoliation (EOR)). Then the trends of the four phenology metrics from 2003 to 2022 in the northern edge of Asian tropics were explored. Finally, the phenological responses to climatic and topographical factors were also investigated. Results indicated that the kernel normalized difference vegetation index performed best in extracting SOD and EOD while the near-infrared reflectance of vegetation performed best for SOR and EOR. SOD exhibited an annual delay of 0.14 days, whereas EOD, SOR, and EOR showed significantly advance by 0.11, 0.27, and 0.52 days, respectively. The four phenological metrics generally delayed with increasing elevation and slope, with 0.13 days/50 m and 0.21 days/° for SOD, 0.43 days/50 m and 0.24 days/° for EOD, 1.10 days/50 m and 0.31 days/° for SOR, and 0.94 days/50 m and 0.36 days/° for EOR. Temperature and humidity were found to jointly regulate SOD and SOR, while humidity predominantly influenced EOD and EOR. This study contributes to a deeper understanding of the mechanism underlying rubber phenology and its response to future climate change.

1. Introduction

Hevea brasiliensis, commonly known as the rubber tree, is an evergreen broadleaf species in native Amazon tropical regions (Ahrends et al., 2015; Azizan et al., 2023; Chen et al., 2022; George et al., 2009; Priyadarshan, 2011; Wang et al., 2023a). However, after being introduced to Asia, rubber trees exhibit deciduous behavior (within 2 weeks) during the dry season and leaf-flushing (not exceed 4 weeks) before the arrival of the rainy season (Chen et al., 2015; Liyanage et al., 2019; Chen et al., 2022). Mapping the spatiotemporal variations of rubber phenology and exploring its controlling mechanisms in introduced regions can enhance our understanding of the interactions between rubber plantations and climate (Piao et al., 2006; Melaas et al., 2013; Liu et al., 2016). Nevertheless, our current understanding of rubber phenology and its driving mechanisms remains insufficient.

Currently, research on rubber plantation phenology primarily relies on ground-based data to understand basic phenological patterns. For instances, Zhai et al. (2019) found that rubber leaf flushing primarily occurred from February to March based on 22 observational sites. Gutiérrez-Vanegas et al. (2020) found that defoliation started in the final weeks of current year and refoliation started during February to March in three rubber tree clones in Colombia. Lai et al. (2023) found that defoliation was delayed by 0.38 days/year, while refoliation was advanced by 0.94 days/year from 2001 to 2020 based on 32

* Correspondence to: School of Geographical Sciences, Fujian Normal University, China.
E-mail addresses: qsx20221108@student.fjnu.edu.cn (Y. Chen), nuttapon.k@cmu.ac.th (N. Khongdee), sqh@xtbg.ac.cn (Q. Song), ludengsheng@finu.edu.cn (D. Lu), shusen.wang@canada.ca (S. Wang), chenyl@fjnu.edu.cn (Y. Chen).

https://doi.org/10.1016/j.indcrop.2025.120753
Received 6 September 2024; Received in revised form 17 February 2025; Accepted 19 February 2025
Available online 24 February 2025

observational sites in Yunnan Province, China. However, these site-specific research findings are difficult to extrapolate to larger region due to their scale limitations. The temporal patterns of rubber plantation phenology still remain unclear at large spatial scale. In addition, though quite a lot studies have investigated the main drivers of rubber phenology, there is still debate on the reason for rubber leaf defoliation. Guerra-Hincapié et al. (2020) found that rainfall was the most critical factor triggering leaf defoliation, while Lin et al. (2018), Azizan et al. (2023) and Lai et al. (2023) found that temperature was more strongly associated with leaf defoliation. Meanwhile, Guardiola-Claramonte et al. (2010) suggested that temperature, vapor pressure deficit and day length jointly influenced rubber defoliation. A significant reason for the inconsistency in these findings is that most studies are limited to site-specific scales or short-term study periods. Therefore, it is urgently needed to investigate the relationship between rubber plantation phenology and meteorological factors at larger spatial scales and long-term periods to identify the primary drivers of rubber plantation phenology.

Remote sensing provides obvious advantages over traditional ground-based inventories for monitoring phenology across large spatial and long temporal scales (Jeong et al., 2017; Piao et al., 2019). Vegetation indices (VIs) were extensively used in remote sensing to retrieve surface phenology. Among them, the Normalized Difference Vegetation Index (NDVI) (Tucker, 1979) and the Enhanced Vegetation Index (EVI) have been the two most commonly employed indices over the past few decades (Zhang et al., 2003; Fu et al., 2015; Berra et al., 2021). Recently, the near-infrared reflectance of vegetation (NIRv) (Badgley et al., 2017) and the kernel NDVI (kNDVI) (Camps-Valls et al., 2021) have emerged as new VIs. NIRv is widely used due to its ability to mitigate the influence of soil effects and background brightness (Badgley et al., 2017). kNDVI, with its higher sensitivity to plant physiological and physical parameters compared to NDVI, shows great potential for phenology studies (Camps-Valls et al., 2021). Due to the varying spectral responses of canopy biochemistry to different bands, VIs composed of different spectral bands often result in variations in the derived phenology dates (Zeng et al., 2020). For example, Peng et al. (2017) found that EVI performed better than NDVI in extracting spring phenology. Zhang et al. (2022) compared NIRv, NDVI, and EVI across six types of plantations and found that NIRv performed best in phenology monitoring. However, the performance of NDVI, EVI, NIRv, and kNDVI in extracting rubber phenology remains unassessed. Thus, it is unclear which of these four indices performs best for extracting rubber phenology.

In recent decades, climate change has significantly altered global spatiotemporal patterns and trends in vegetation phenology, including the widely reported advancement of spring phenology and the delay of autumn phenology (Guyon et al., 2011; Melaas et al., 2013; Piao et al., 2019; Berra and Gaulton, 2021). However, phenology studies are limited for tropical tree species, especially for rubber trees (Richardson et al., 2010). In introduced rubber plantation areas, such as southwestern China and Southeast Asia, rubber phenology is characterized by early occurrences and short cycles. For example, leaf shedding and leaf flushing phases typically occur within 2 weeks, while the leafless period usually does not exceed 4 weeks. This makes it challenging to accurately extract rubber phenology in tropical regions with frequent cloud cover and rainfall. Therefore, this study aims to accurately map four rubber phenological metrics (i.e., Start of Defoliation (SOD), End of Defoliation (EOD), Start of Refoliation (SOR), End of Refoliation (EOR)) and investigate their temporal-spatial patterns and driving mechanisms. Specifically, this study seeks to answer the following questions:

(1) Which is the best vegetation index among NDVI, EVI, NIRv, and kNDVI in monitoring rubber phenology? And what is the optimal threshold?
(2) What are the spatial patterns and temporal trends of the four rubber phenological dates?
(3) What are the primary topographic and climatic factors affecting each rubber phenological event? And how do they influence these events?

2. Study area and methods

2.1. Study region

Xishuangbanna is China's largest city-level region for natural rubber plantations (Fig. 1). Since rubber plantations were introduced in the 1950s, their area has reached approximately 300,821 ha by 2022 (National Bureau of Statistics of China, 2023). Influenced by the southeast trade winds from the Pacific Ocean and the southwest monsoon from the Indian Ocean, the study area has distinct rainy (May to October) and dry seasons (November to April) (Lin et al., 2018). During the dry season, rubber trees undergo a rapid leaf-exchange process (leaf shedding and regrowth) to better facilitate growth and rubber production in rainy season (Wang et al., 2023a; Xiao et al., 2019).

2.2. Data and preprocessing

2.2.1. Vegetation indices

Two MODIS reflectance products, MOD09GA and MOD09QA, derived from the NASA USGS Data Center, were used to generate the four VIs (NDVI, EVI, NIRv, and kNDVI, calculated according to Eqs. (1) - (5)) from 2003 to 2022. Daily red and near-infrared surface reflectance with a spatial resolution of 250 m were obtained from the MOD09GQ product. Additionally, blue surface reflectance with a 500 m resolution and the state_1km_1 band (QA flag information) with a 1 km resolution were obtained from the MOD09GA product. Note that the blue and state_1km_1 bands were resampled to 250 m. Subsequently, poor-quality pixels were masked to reconstruct the complete VI time series, using the state_1km_1 band, which provides information about the atmospheric conditions (Vermote et al., 2015).

$$\mathrm{NDVI} = \frac{NIR - R}{NIR + R} \tag{1}$$

$$\mathrm{EVI} = 2.5 \times \frac{NIR - R}{NIR + 6 \times R - 7.5 \times Blue + 1} \tag{2}$$

$$\mathrm{NIRv} = \left(\frac{NIR - R}{NIR + R} - 0.08\right) \times NIR \tag{3}$$

$$\mathrm{kNDVI} = \frac{k(NIR, NIR) - k(NIR, R)}{k(NIR, NIR) + k(NIR, R)} \tag{4}$$

$$\mathrm{k(a, b)} = \exp\left(- (\mathrm{a} - \mathrm{b})^2 \div (2\sigma^2) \right) \tag{5}$$

where R is the reflectance of the red band, NIR is the reflectance of the near-infrared band, $Blue$ is the reflectance of the blue band, and σ is a length-scale parameter.

2.2.2. Annual rubber plantation maps

The annual rubber maps (2003–2022) with a spatial resolution of 30 m were derived from Xu et al. (unpublished data, 2025). In Google Earth Engine, Xu et al. introduced a new framework for mapping time series rubber distribution using a random forest classifier, integrating spectral data, topography, dynamic phenological VIs, dynamic texture features, and change detection features. The average overall accuracy from 1987 to 2022 is 90.82 %, and the kappa coefficient is 0.89. To align with the spatial resolution of MODIS, all rubber maps were resampled to 250 m. Specifically, the resampled 250-meter pixel containing over 90 % of 30-meter rubber pixels was reclassified as rubber plantation.

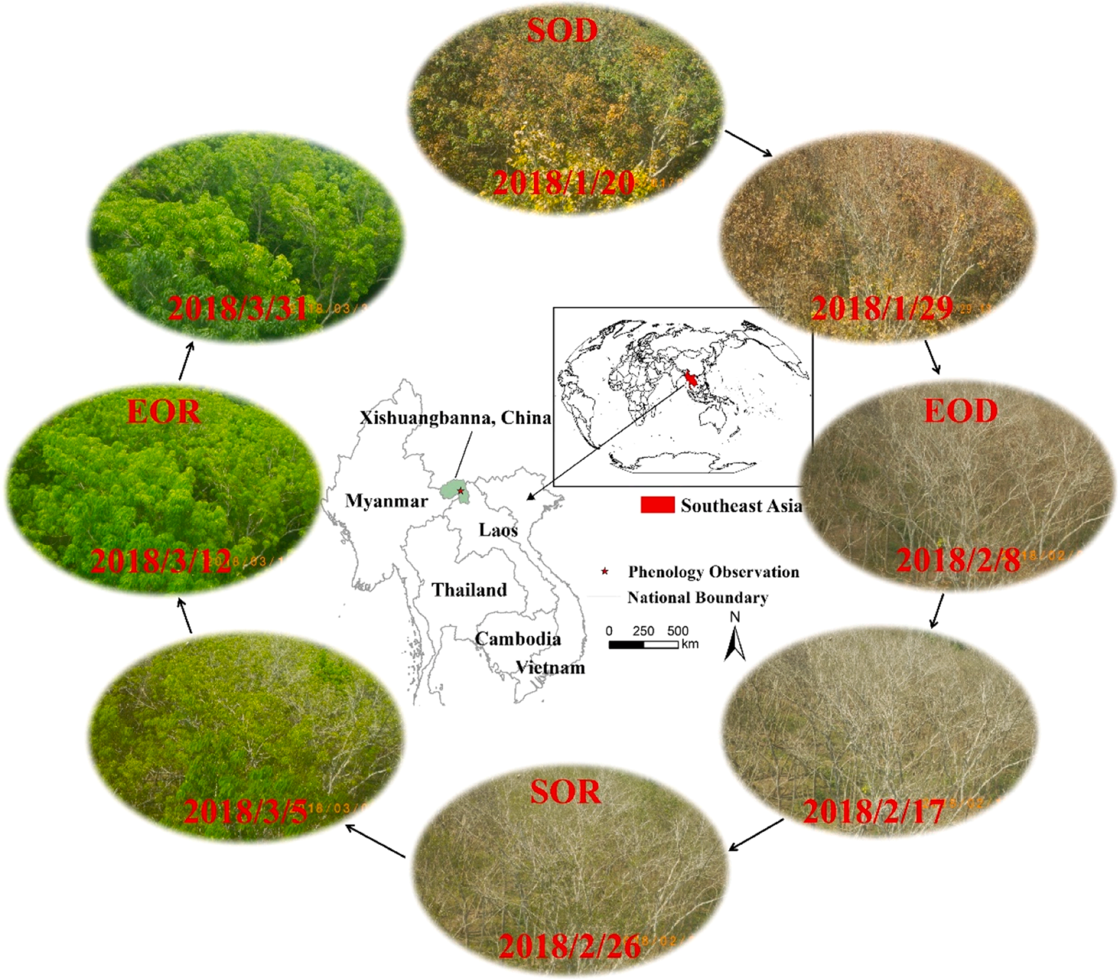

Fig. 1. Rubber phenology development and the location of study region.

2.2.3. *Phenological observation data*

Ground-based phenological observation data from 2012 to 2022 were obtained from a phenology camera installed at the top of Xishuangbanna flux tower, which recorded the defoliation, sprouting, growth, and leaf spreading of rubber trees (Zhou et al., 2019). The camera was mounted on a tower 30 m above the ground, with the lens facing southwest at an inclination of 57°. Images disturbed by rain or fog were then excluded. Finally, the highest-quality images were selected for subsequent phenological metrics determination. Within each image, we visually determined the date of four phenological metrics by observing the state changes in a fixed region of interest.

2.2.4. *Climatic data*

The Xishuangbanna Ecological Research Station provided the daily climatic data from 2002 to 2018, including maximum temperature (Tmax, unit: °C), minimum temperature (Tmin, unit: °C), photoperiod (unit: hours), relative humidity (RH, unit: %), and vapor pressure deficit (VPD, unit: kPa). The station is located within the Xishuangbanna Tropical Botanical Garden of Chinese Academy of Sciences (101°16′E, 21°55′N) (Fig. 1). Considering the uniform environment within a small area, this study selected rubber pixels within 500 m of the station to analyze the main driving climate factors on rubber phenology. Previous studies have demonstrated that climate variations over a three-month advance significantly impact the phenological metrics (Menzel et al., 2006). Therefore, we investigated the driving mechanism of meteorological factors at nine time periods, from 10 to 90 days before the phenological dates with 10-day intervals.

2.2.5. *Topographic data*

The AW3D30DEM Version 4.0 product was provided by the Japan Aerospace Exploration Agency (JAXA) with a horizontal resolution of 30 m (1 arc second) and an elevation accuracy of 5 m (Takaku et al., 2020). Compared to SRTM and GDEM2, AW3D30DEM has been proven to have better vertical accuracy (Li et al., 2018). To match the MODIS data, we resampled it to 250 m using the bilinear interpolation method. The altitude, slope, and aspect values were then extracted to explore their influence on rubber plantation phenological metrics. Table 1.

Table 1
Data used in the study.

Data Type	Spatiotemporal Resolution	Time Span	Data Source
MOD09GQ, MOD09GA	250 m, daily	2002–2022	http://www.nasa.gov/
Annual rubber plantation maps	30 m, yearly	2002–2022	Xu et al. (unpublished data, 2025)
Phenological observation data	daily	2012–2022	Zhou et al. (2019)
Climatic data	daily	2002–2018	http://www.nesdc.org.cn/
AW3D30DEM	30 m	2006–2011	https://www.eorc.jaxa.jp/ALOS/en/dataset/aw3d30/

2.3. Methods

Fig. 2 showed the detailed research process, including the following 4 steps: (1) reconstructing daily time series of four vegetation indices; (2) extracting the spatiotemporal distribution of the four rubber phenological metrics; (3) analyzing the spatiotemporal patterns of the four rubber phenological metrics; and (4) exploring the impact mechanism of climate on the four rubber phenological metrics.

2.3.1. Reconstructing vegetation indices time-series

Due to the frequent cloud cover and rainy weather in the study area, anomalies and missing values often occur in time series imagery (Atkinson et al., 2012), which can significantly interface with the accurate extraction of phenological dates. Therefore, it is necessary to remove noise and interpolate missing values to ensure a complete and smooth time series that can accurately capture phenological changes (Cui et al., 2021). This study proposed a step-by-step processing flow for identifying and filling noise values based on temporal and spatial neighboring pixels (Fig. 3). Firstly, the VIs time series were preprocessed by removing pixels contaminated by clouds and shadows (Step 1 in Fig. 3). Only pixels with QA flags indicating no contamination were considered. Next, missing values were gap-filled using a temporal interpolation algorithm. Specifically, each missing pixel was filled using the mean value of adjacent dates: one from the front and another from the behind the missing value day in the time series (Step 2 in Fig. 3). Third, if gaps remained, the remaining missing values were further filled using the average value from all high-quality rubber pixels within the interaction region of 50 m elevation buffer zone of the target pixel with initial searching distance starting from 2.5 km (Step 3 in Fig. 3). The search distance would be expanded from 2.5 km to the maximum with 2.5 km interval until the replacing values (at least 2 values) were found.

2.3.2. Extracting phenology metrics

We defined four key phenological metrics as follows:

(1) Start of Defoliation (SOD): The date when the rubber plantation transitions from a stable growth phase to defoliation, marked by a slight decrease in vegetation index (VI) curve.
(2) End of Defoliation (EOD): The earliest date when the VI curve drops to a relatively stable low level.
(3) Start of Refoliation (SOR): After a short leafless period, the date when the VI curve begins to increase significantly from a stable low level.
(4) End of Refoliation (EOR): The date when the VI curve reaches a stable level after SOR.

To obtain a smooth curve for extracting phenological metrics, it is necessary to eliminate fluctuations in the VI time series caused by processing uncertainties and to apply filtering and fitting algorithms. First, the annual VI time series was reconstructed for each rubber plantation target pixel using the maximum of sliding window of size 5. Then, the reconstructed VI time series was further smoothed using Savitzky-Golay (SG) filtering (Savitzky et al., 1964). Additionally, since these four phenological dates primarily occur from the previous December to the current April, we applied mean smoothing to the VI data outside this phenological period (specifically, the previous October and November and the current May, as the period from June to September was not used). This step helps mitigate the influence of large fluctuations in non-phenological periods on the subsequent phenological curve fitting and metrics extraction. The specific implementation is detailed in Eq. (6):

$$\mathrm{Rubber\_TS}_i = mean\left(Rubber_{TS\,day_{Dec.\sim Apr.}}\right) \tag{6}$$

where $\mathrm{Rubber\_TS}_i$ refers to the VI value on day i in the non-phenological period (i.e., the previous October and November and the current May). $Rubber\_TS_{day_{Dec.\sim Apr.}}$ refers to the daily VI values during the phenological period (i.e., from the previous December to the current April).

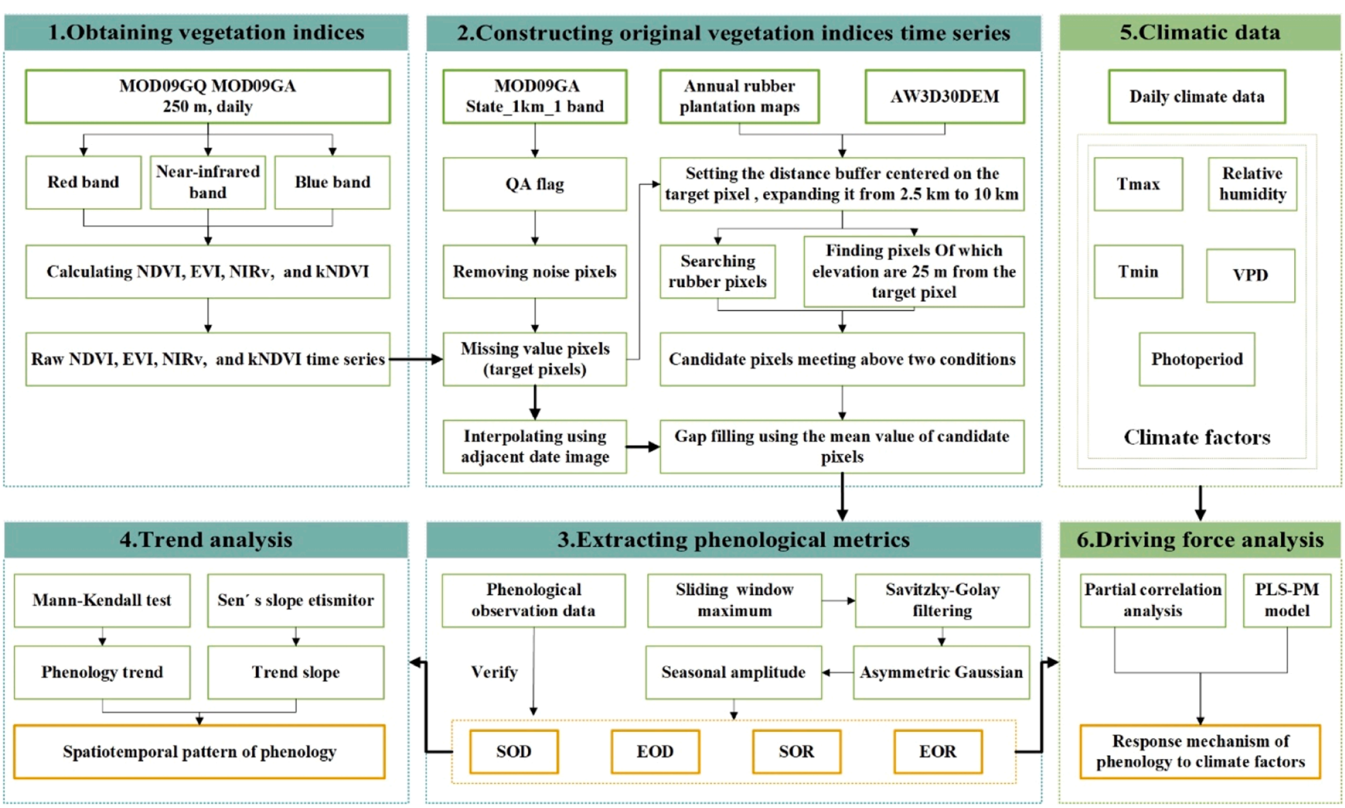

Fig. 2. The flowchart of this study.

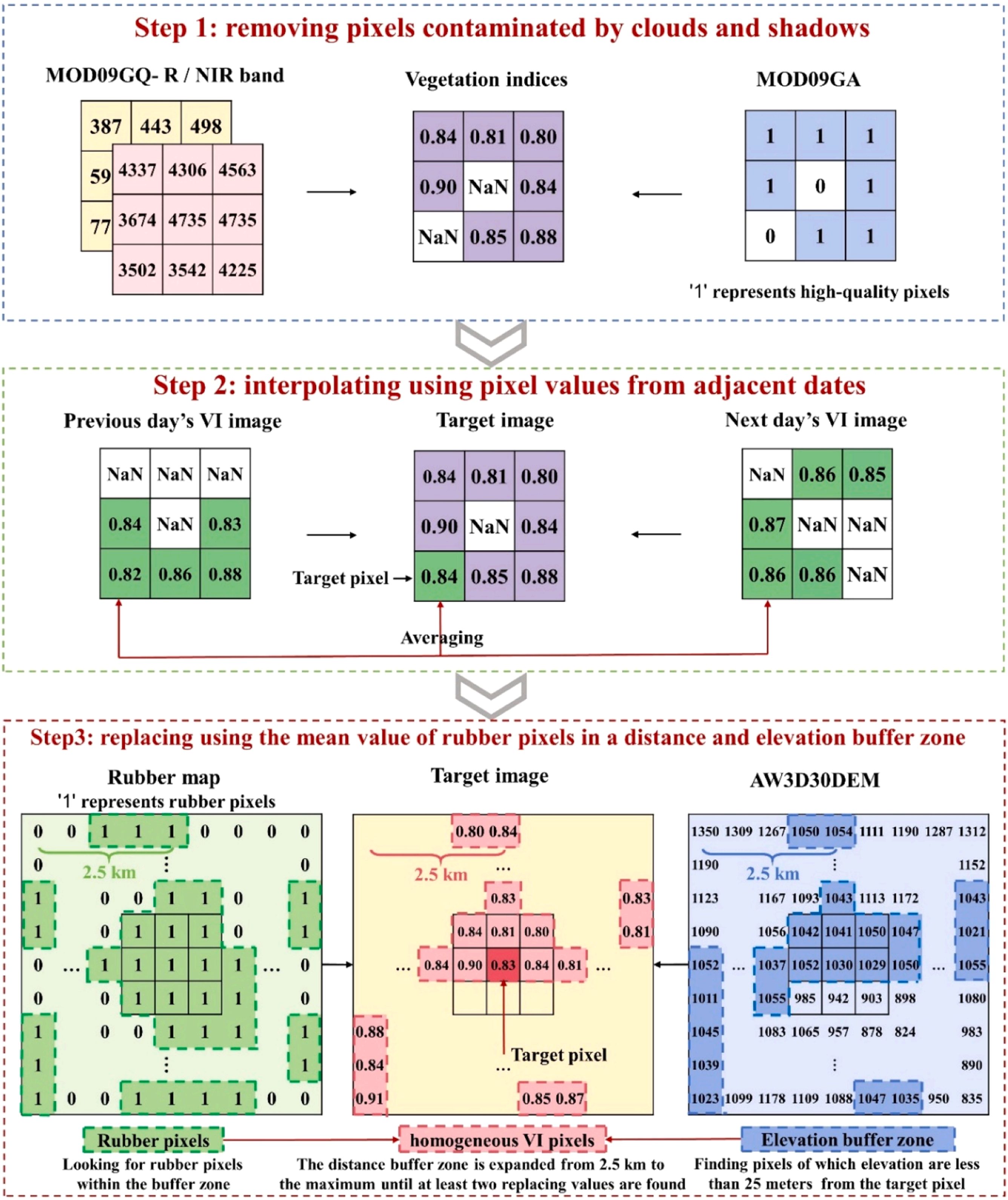

Fig. 3. Step by step flow of spatiotemporal interpolation for the missing values.

Subsequently, curve fitting was performed using the Asymmetric Gaussian (AG) fitting algorithm (Jonsson et al., 2002), as detailed in Eq. (7).

$$\mathrm{Rubber}_{\mathrm{TS}i} = \begin{cases} \exp\left[-\left(\dfrac{i-a_1}{a_2}\right)^{a_3}\right] \; if\ i > a_1, \\ \exp\left[-\left(\dfrac{a_1-i}{a_4}\right)^{a_5}\right] \; if\ i < a_1 \end{cases} \tag{7}$$

where a_1 refers to the position of the maximum or minimum relative to the time variable i. a_2 and a_3 refer the width and steepness of the right side of the function. a_4 and a_5 refer the width and steepness of the left side.

Finally, four rubber phenological metrics were extracted annually using the seasonal amplitude method, implemented with TIMESAT software package (Jönsson and Eklundh, 2004). Previous studies have faced controversy over the determination of thresholds for extracting defoliation and refoliation phenology (Shen et al., 2024). Therefore, this study tested four different thresholds of 5 %, 10 %, 15 %, and 20 % to determine the optimal threshold for SOR and SOD. Similarly, thresholds of 80 %, 85 %, 90 %, and 95 % were explored to identify the optimal threshold for EOR and EOD.

2.3.3. Trend analysis

Trends of the four phenological metrics were examined using the Theil-Sen estimator and the Mann-Kendall significance test for each rubber pixel. The Theil-Sen slope is a robust nonparametric method for trend analysis that is resistant to outliers (Sen, 1968). The Mann-Kendall test (Mann, 1945) has been widely applied in recent years to assess the significance of trends in vegetation and climate variables.

2.3.4. Driving force analysis

(1) Partial correlation

To compare the phenological response to climatic factors, partial correlation analysis was separately calculated for the 10–90 days preceding each phenological date.

(2) Structural equation model

In this study, we used Partial Least Squares Path Modeling (PLS-PM) to analyze the linear statistical relationships among multiple variables. PLS-PM is one kind of Structural Equation Modeling estimation methods, especially suitable for small samples sizes and data with non-normal distribution (McIntosh et al., 2014). The path model was constructed by two categories of latent variables: temperature latent variables (i.e., Tmax and Tmin) and humidity latent variables (i.e., VPD and RH), clarifying the influence mechanism of rubber phenology.

3. Result

3.1. Evaluation of four vegetation indices on extracting rubber phenology

Evaluation of the four vegetation indices and different thresholds for extracting phenological metrics revealed the following findings (Fig. 4 and Table 2): (1) kNDVI performed best on extracting SOD (RMSE=6.80 days) with the optimal threshold of decreasing 20 %, followed by NDVI with RMSE of 10.70 days by using its optimal threshold of decreasing 10 % (Fig. 4a and Table 2). (2) Both kNDVI and NDVI showed good performance on extracting EOD with no significant difference on RMSE (5.90 and 5.80 days, respectively) (Fig. 4b). The optimal threshold of kNDVI and NDVI was same with 95 % decreasing for extracting EOD. (3) NIRv performed best on extracting SOR (RMSE=2.50 days) with the optimal threshold of increasing 10 %, followed by EVI with RMSE of 3.10 days by using its optimal threshold of increasing 5 % (Fig. 4c and Table 2). (4) Both NIRv and NDVI showed good performance on extracting EOR with no significant difference on RMSE (5.00 and 5.30 days, respectively) (Fig. 4d). The optimal threshold of NIRv and NDVI was same with 90 % increasing for extracting EOR (Table 2).

3.2. Spatiotemporal patterns of the four rubber phenological dates

3.2.1. Temporal variation of rubber phenological dates

Fig. 5 showed the temporal variation of four rubber phenological dates based on their optimal VIs (i.e., kNDVI for SOD and EOD, and NIRv for SOR and EOR). The SOD was mainly concentrated in January, with over 70 % of occurred rubber pixels. The EOD mainly occurred at the period between the latter half of January and the first half of February

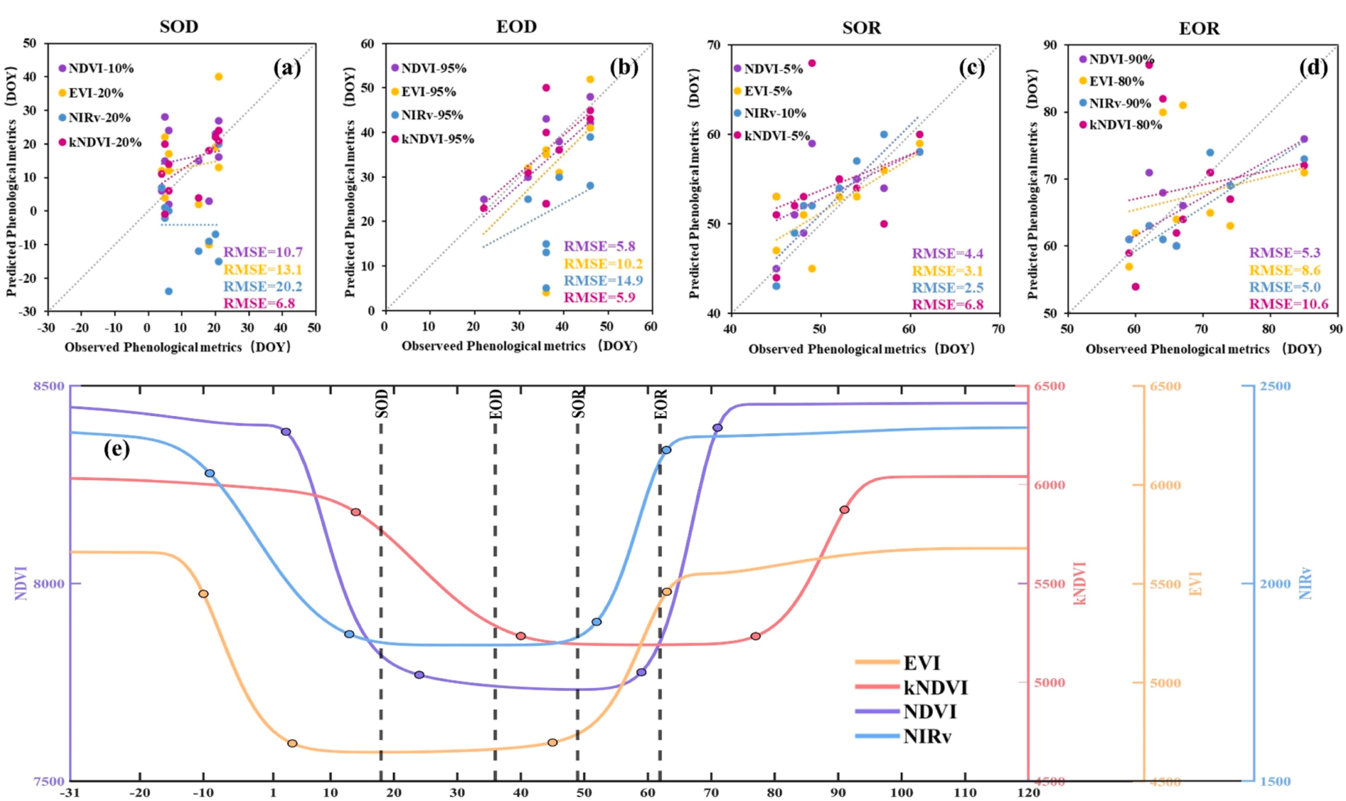

Fig. 4. Evaluation of four vegetation indices (NDVI, EVI, NIRv, and kNDVI) on extracting rubber phenology: (a) SOD, (b) EOD, (c) SOR, (d) EOR, (e) predicted (colored cycles) and observed (vertical dash line) phenology dates on the time series of the four VIs.

Table 2
Root mean square error of different thresholds for each vegetation index.

RMSE (Days)	NDVI				NIRv			
	5 %	10 %	15 %	20 %	5 %	10 %	15 %	20 %
SOD	13.67	**10.74**	11.45	12.09	32.13	25.75	22.40	**20.21**
EOD	**5.81**	7.41	8.30	9.39	**14.88**	17.31	19.05	20.51
SOR	**4.36**	4.81	5.66	6.12	2.56	**2.49**	3.06	3.64
EOR	6.45	**5.26**	5.68	6.02	12.70	**4.98**	5.60	6.16
RMSE (Days)	**EVI**				**kNDVI**			
	5 %	10 %	15 %	20 %	5 %	10 %	15 %	20 %
SOD	24.17	15.55	13.51	**13.11**	29.85	9.21	6.91	**6.80**
EOD	**10.23**	11.36	11.99	12.92	**5.85**	6.15	6.64	7.48
SOR	**3.07**	4.10	4.95	5.85	**6.79**	7.93	8.76	9.50
EOR	26.56	11.85	9.56	**8.62**	15.79	12.53	11.42	**10.57**

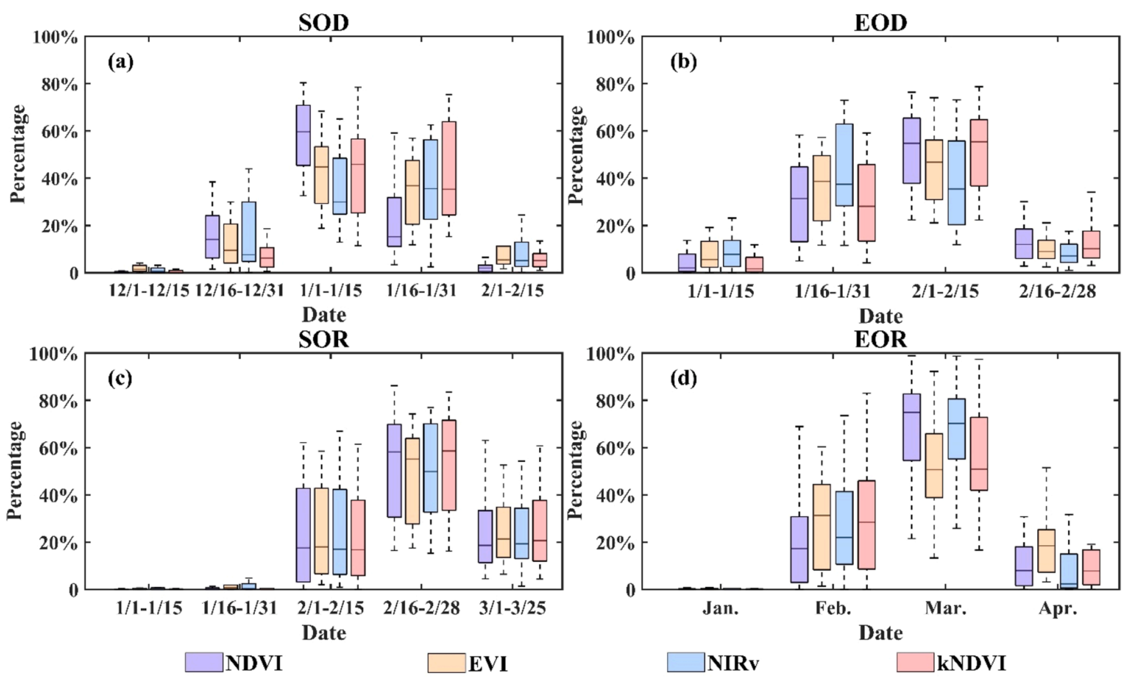

Fig. 5. Percentage distribution of the four rubber phenology dates derived by different vegetation index: (a) SOD; (b) EOD; (c) SOR; (d) EOR.

(over 80 % of rubber pixels). The SOR primarily occurred in February (over 70 % of rubber pixels), while the EOR mainly occurred in March (over 80 % of rubber pixels). It is worth noting that NDVI generally estimated SOD with 4.86 days earlier than other three VIs while NIRv estimated EOD with 3.66 days earlier than other three VIs. There are no significant differences in the temporal variation of SOR estimated by the four VIs. However, NIRv tended to estimate EOR earlier than other three VIs with 3.65 days.

3.2.2. *Spatiotemporal patterns of rubber phenological dates*

Trend analysis was conducted on three scales: the entire study area, low-altitude regions (600–800 m), and high-altitude regions (800–1000 m). Results of these three scales indicated that EOD, SOR, and EOR showed consistent advanced trends regardless of which VI was used and advanced trends of the latter two refoliation dates were significant at $\alpha = 0.05$ level (Fig. 6d-l). The average advancement trends of all VIs for EOD, SOR, and EOR were 0.13, 0.34, and 0.66 days per year, respectively, across the entire study area (Fig. 6d, g, and j). The advancement trends of the optimal VI for EOD, SOR, and EOR were 0.11, 0.27, and 0.52 days per year, respectively, across the entire study area (Fig. 6d, g, and j). Although EOD showed advanced trend on all the VIs, there was basically no significant (Fig. 6d-f). The maximum advanced rate gap of EOD was only 0.18, 0.26 and 0.36 days per year for the four VIs at the three scales respectively (Fig. 6d-f). In contrast, considerable advanced rate gaps can be found on SOR and EOR at all the three scales.

The VI with minimum and maximum advanced trends differed on each phenological date. For EOD, NDVI had minimum advanced rate while EVI owned the maximum at all three scales (Fig. 6d-f). For SOR, NIRv had the minimum advanced rate while EVI dominated the maximum (Fig. 6g-i). For EOR, NIRv also had the minimum advanced rate while kNDVI had the maximum at all three scales (Fig. 6j-l). It can also be obviously observed that the advanced rate of refoliation phenology (SOR and EOR) was much larger than that of defoliation phenology (EOD) at all three scales. In contrast to the consistent advanced trend of EOD, SOR and EOR, SOD exhibited opposite trends among different VIs. For example, across the entire study area, EVI- and NIRv-based SOD showed advancement trends of 0.40 and 0.42 days per year, respectively, whereas NDVI and kNDVI exhibited opposite trends with delays of 0.04 and 0.14 days per year, respectively (Fig. 6a). However, only EVI-based SOD showed a significant trend (α=0.05) among the four VIs (Fig. 6a-c).

Fig. 7 showed the spatial pattern of temporal trends of the four phenological dates based on their corresponding optimal index and threshold. Dominated delayed trend can be observed in SOD while

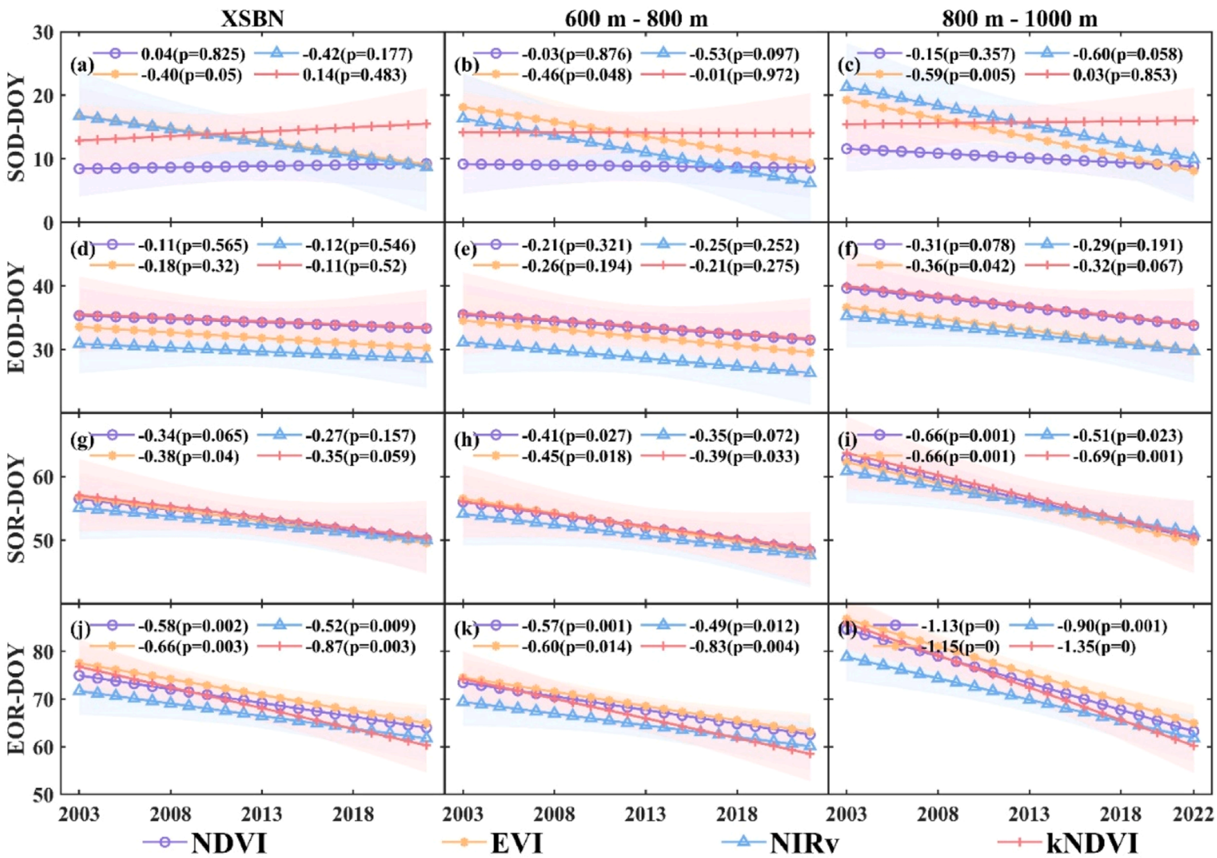

Fig. 6. Rubber phenology dates trend derived by each vegetation index at three scales.

dominated advanced trend can be observed in EOD, SOR and EOR. Specifically, 65.09 % of rubber pixels showed delayed trend in SOD, in which 7.19 % of pixels were significant. Over 74.01 % of rubber pixels exhibited advanced trends in EOD, with 18.54 % of pixels being significant. Over 74.61 % of rubber pixels exhibited advanced trends in SOR (22.44 % significantly). The spatial pattern of advanced trends in EOR was the most pronounced, with approximately 85.91 % pixels exhibiting advanced trends (35.52 % significantly).

3.3. Relationship between topographical factors and rubber phenology

The four phenological dates generally showed delayed trend with arising elevation (Fig. 8 and Table 3). Taking the optimal index based phenology as example, 60 %, 85 %, 100 % and 75 % of years showed delayed trend with arising elevation in kNDVI-based SOD and EOD, and NIRv-based SOR and EOR, respectively (Table 3). Among all the delayed years, around 67 %, 76 %, 95 % and 80 % of years were significant at $\alpha = 0.05$ (Table 3). The SOD, EOD, SOR, and EOR based on the four VIs were averagely delayed by 0.27 days/50 m, 0.44 days/50 m, 0.72 days/50 m, and 0.91 days/50 m, respectively. The SOD, EOD, SOR, and EOR based on the optimal VI (namely kNDVI-based SOD and EOD, and NIRv-based SOR and EOR) were averagely delayed by 0.13 days/50 m, 0.43 days/50 m, 1.10 days/50 m, and 0.94 days/50 m, respectively. Notably, the delayed rates of refoliation phenological dates were generally larger than that of defoliation phenological dates. For example, the average delayed rate of EOR based on four VIs was 0.64 and 0.47 days larger than that of SOD and EOD, respectively (Fig. 8a, b, and d). The delayed rate gaps among different VIs were not consistent on the four phenological dates (Table 4). Multi-comparison results indicated that the delayed rate differences between NIRv and the other three VIs were significant on SOD and EOD (Table 4), as also be reflected in their large gaps shown in Fig. 6. Interestingly, the delayed rate gaps between kNDVI and NDVI were relatively small in all four phenological dates (Fig. 8). Multi-comparison results also confirmed that their differences were no significant (Table 4).

The four phenological dates generally showed delayed trend with arising slope regardless of the type of VI used (Fig. 9 and Table 3). Taking the optimal index based phenology as example, 90 %, 95 %, 90 % and 90 % of years showed delayed trend with arising slopes in SOR and EOR, respectively (Table 3). Among all the delayed years, around 89 %, 84 %, 94 % and 89 % of years were significant at $\alpha = 0.05$ (Table 3). On average, SOD, EOD, SOR, and EOR based on the four VIs were delayed by 0.19 days/°, 0.22 days/°, 0.32 days/°, and 0.50 days/°, respectively. The SOD, EOD, SOR, and EOR based on the optimal vegetation index were averagely delayed by 0.21 days/°, 0.24 days/°, 0.31 days/°, and 0.36 days/°, respectively. Unlike the results of elevation, the delayed rate gaps among different VIs were generally small (Table 4). Multi-comparison results indicated that the delayed rate differences between most VIs were not significant (Table 4). The only significant delayed rate gaps were found between EVI and other VIs for SOD and EOD (Table 4).

Examination of the relationship between phenological metrics and different aspects (Fig. 10) revealed that aspect had minimal impact on rubber plantation phenology. It is evident that the phenological dates on sunny slopes were very close to those on shaded slopes, regardless of the type of phenology metrics and VIs. A comparison test at a 95 % confidence level (Table 4) also confirmed that there were no significant differences among phenological dates on sunny and shaded aspects.

3.4. Influence of climate change on rubber phenology

3.4.1. Correlation between phenology and climatic factors

Tmax, Tmin, RH, and VPD exhibited higher and significant correlations with the four rubber phenological metrics, whereas photoperiod

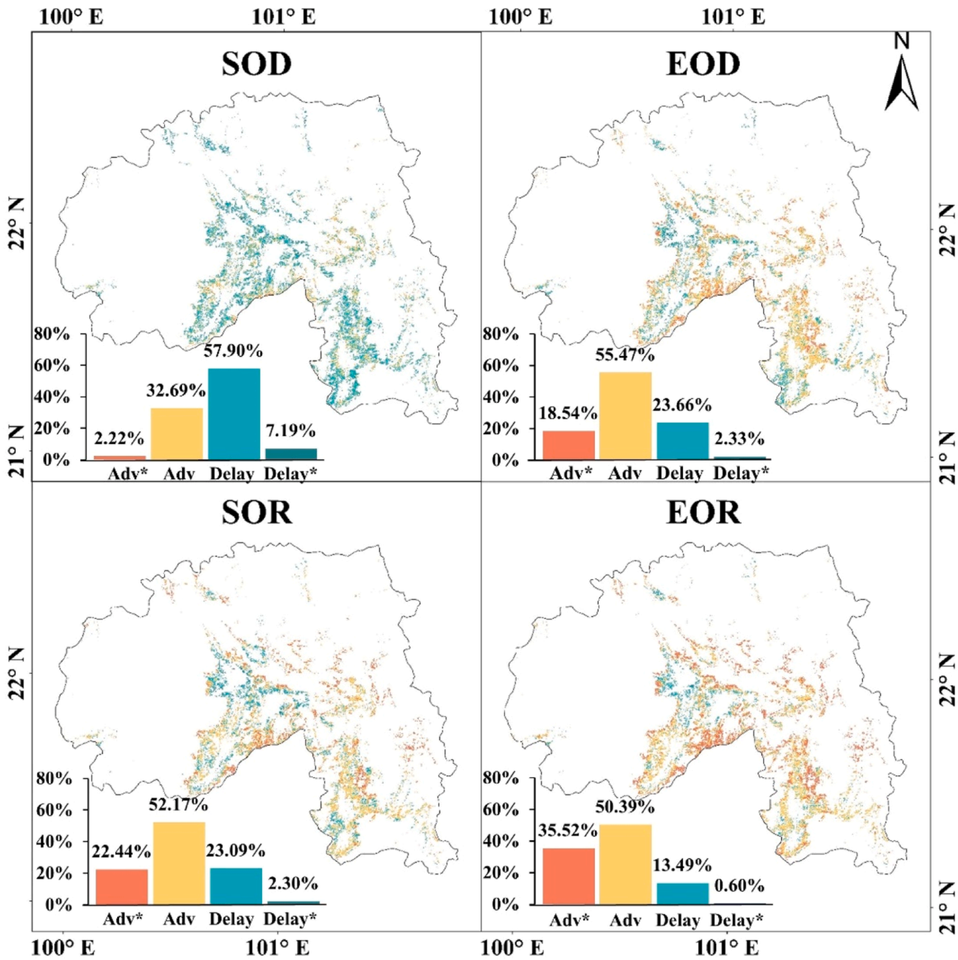

Fig. 7. Spatial distribution of rubber phenology trend (a) SOD, (b) EOD, (c) SOR, and (d) EOR from 2003 to 2022. The bar chart shows the percentage of advanced and delayed trends of all rubber pixels. 'Adv' represents the advancing trend, 'Delay' represents the delayed trend, and '* ' represents the significant level at $\alpha = 0.1$.

showed lower or non-significant correlations (Fig. 11). Tmax, Tmin, and RH showed positive partial correlations with SOD while negative partial correlations with EOD, SOR, and EOR. Tmin and Tmax demonstrated higher partial correlations with SOD compared to RH and VPD, whereas RH and VPD showed larger and more stable partial coefficients with EOD, SOR, and EOR. It should be noted that the climatic correlations with EOD were generally low, with the maximum correlation being less than 0.4, suggesting that the drivers of EOD were complex. We also found that the main climate influencing periods of the four phenological dates differed. The main climate influencing periods of SOD and EOD were from 60 to 90 days and 20–50 days before their occurrence respectively. The main climate influencing periods of SOR and EOR were from 20 to 60 days and 40–70 days before their occurrence respectively. During these main influencing period, VPD showed the largest partial correlation with SOD (mean PCCs = −0.57), followed by Tmax. VPD showed the largest partial correlation with EOD (mean PCCs = −0.31), followed by Tmin. RH exhibited the largest partial correlation with SOR (mean PCCs = −0.53), followed by VPD. VPD showed the largest partial correlation with EOR (mean PCCs = 0.67), followed by RH. The above results implied that both temperature latent variables (Tmax and Tmin) and humidity latent variables (RH and VPD) may co-control SOD, while humidity latent variables may primarily affect SOR and EOR.

3.4.2. *Drivers of each rubber phenological metric*

Path analysis also revealed that temperature latent variables (Tmax and Tmin) and humidity latent variables (RH and VPD) had comprehensive influences on SOD and SOR, while humidity latent variables primarily affected EOD and EOR (Table 5). Specifically, the path coefficients of humidity latent variables outweighed those of temperature latent variables during 70–90 days preceding SOD occurrence and the loading values of VPD were much higher than RH, highlighting VPD as the primary climatic factor influencing SOD. In other words, higher VPD promoted earlier SOD occurrence. Conversely, the path coefficients of temperature latent variables exceeded those of humidity latent variables during 10–60 days preceding SOD occurrence, with Tmax having much higher loading values than Tmin. This highlighted Tmax as the primary climatic factor influencing SOD, where lower Tmax promoted earlier SOD occurrence. Path coefficients of humidity latent variables consistently outweighed those of temperature latent variables during 10–90 days preceding EOD occurrence, with RH generally having higher loading values than VPD. This suggested that RH was the primary climatic factor influencing EOD, although its role may not be decisive due to its relatively small path coefficient.

For SOR, path coefficients of humidity latent variables exceeded those of temperature latent variables during 50–90 days preceding occurrence and the loading values of RH were much higher than VPD, highlighting RH as the primary climatic factor influencing SOR. Namely, higher RH promoted earlier SOR occurrence. However, during the 10–40 days preceding SOR occurrence, path coefficients of temperature latent variables outweighed those of humidity latent variables, with Tmin having much higher loading values than Tmax. This highlighted Tmin as the primary climatic factor influencing SOR, where lower Tmin promoted earlier SOR occurrence. Lastly, path coefficients of humidity latent variables consistently outweighed those of temperature latent

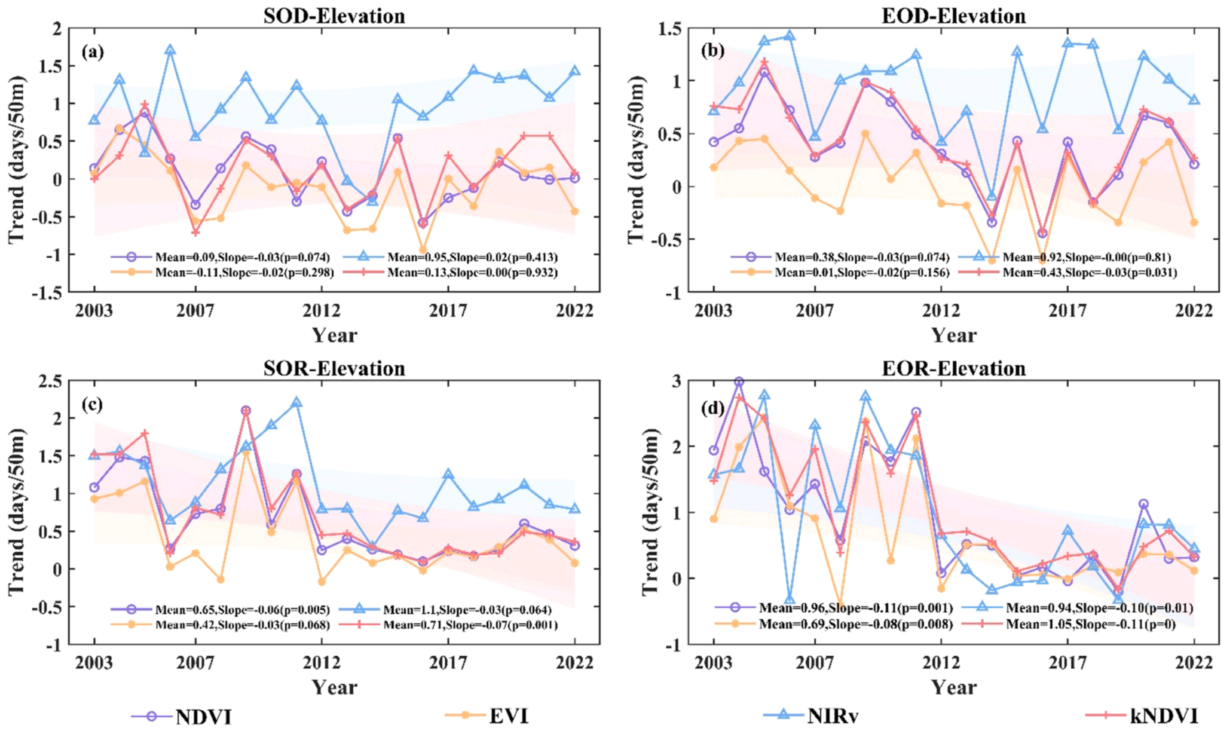

Fig. 8. Rubber phenology trend at different elevations from 2003 to 2022.

Table 3
Percentage of delayed and advanced years for each vegetation index and phenological date.

Phenology metrics	Percentage (%)	NDVI		EVI		NIRv		kNDVI	
		Delayed	Advanced	Delayed	Advanced	Delayed	Advanced	Delayed	Advanced
					Elevation				
SOD	ALL	60 %	40 %	50 %	50 %	90 %	10 %	60 %	40 %
	P < 0.05	50 %	75 %	20 %	70 %	94 %	50 %	67 %	50 %
EOD	ALL	85 %	15 %	55 %	45 %	95 %	5 %	85 %	15 %
	P < 0.05	65 %	67 %	55 %	44 %	95 %	0 %	76 %	100 %
SOR	ALL	100 %	0 %	85 %	15 %	100 %	0 %	100 %	0 %
	P < 0.05	70 %	0 %	47 %	0 %	95 %	0 %	65 %	0 %
EOR	ALL	90 %	10 %	85 %	15 %	75 %	25 %	95 %	5 %
	P < 0.05	72 %	0 %	35 %	0 %	80 %	40 %	79 %	0 %
					Slope				
SOD	ALL	80 %	20 %	65 %	35 %	100 %	0 %	90 %	10 %
	P < 0.05	88 %	75 %	77 %	71 %	85 %	0 %	89 %	100 %
EOD	ALL	95 %	5 %	80 %	20 %	100 %	0 %	95 %	5 %
	P < 0.05	89 %	100 %	88 %	100 %	95 %	0 %	84 %	100 %
SOR	ALL	95 %	5 %	100 %	0 %	90 %	10 %	100 %	0 %
	P < 0.05	100 %	0 %	90 %	0 %	94 %	100 %	95 %	0 %
EOR	ALL	95 %	5 %	100 %	0 %	90 %	10 %	100 %	0 %
	P < 0.05	100 %	0 %	100 %	0 %	89 %	100 %	100 %	0 %

variables during 10–70 days preceding EOR occurrence and the loading values of VPD were generally higher than RH, highlighting VPD as the primary climatic factor influencing EOR. Namely, lower VPD promoted earlier EOR occurrence.

4. Discussion

4.1. Comparison of rubber phenology with previous studies

In this study, the RMSE of extracted SOD, EOD, SOR and EOR are 6.8, 5.9, 2.5, and 5.0 days respectively. This accuracy is higher than most satellite-based phenology studies. This is reasonable as rubber plantations, typically large-scale monocultures, generate more consistent and detectable spectral signals than nature forest with multiple tree species and complex phenological patterns during the occurrence of defoliation or refoliation. The accuracy of our extracted rubber phenology is also higher than other reported rubber phenology studies. For example, our reported RMSE on SOR is around 4 days lower than that (mean difference from comparison with Sentinel-2 observation) reported by Azizan et al. (2021), who utilized the MODIS 8-day time series data whereas this study used daily time series data. Previous studies have also shown that extraction errors for autumn phenology are often larger than those for spring phenology (Zeng et al., 2020; Azizan et al., 2021). For instance, Hmimina et al. (2013) found that the RMSE of spring phenology ranged from 3 to 10 days while that of autumn phenology was much larger, reaching 6–22 days. Similarly, our study also indicates that the extraction accuracy of rubber autumn phenology (SOD and EOD) are lower than that of spring phenology (SOR and EOR). This discrepancy can be

Table 4
Multiple comparisons of vegetation index based on phenological dates at different topographic elements.

Elevation					
Index1	Index2	SOD	EOD	SOR	EOR
NDVI	EVI	0.450	**0.013**	**0.012**	1.000
NDVI	NIRv	**0.003**	**0.000**	**0.006**	1.000
NDVI	kNDVI	1.000	1.000	1.000	0.948
EVI	NIRv	**0.000**	**0.000**	**0.000**	1.000
EVI	kNDVI	0.450	**0.000**	**0.001**	**0.050**
NIRv	kNDVI	**0.003**	**0.029**	0.082	1.000
Slope					
Index1	Index2	SOD	EOD	SOR	EOR
NDVI	EVI	0.726	**0.005**	1.000	0.086
NDVI	NIRv	**0.000**	0.433	1.000	1.000
NDVI	kNDVI	0.210	1.000	1.000	0.224
EVI	NIRv	**0.000**	**0.000**	1.000	**0.002**
EVI	kNDVI	**0.002**	**0.000**	0.559	1.000
NIRv	kNDVI	0.131	1.000	1.000	**0.009**
Aspect					
Aspect1	Aspect2	SOD	EOD	SOR	EOR
NDVI-Sunny	NDVI-Shade	**0.000**	**0.000**	0.655	1.000
EVI-Sunny	EVI-Shade	1.000	0.180	0.655	0.180
NIRv-Sunny	NIRv-Shade	**0.000**	**0.000**	**0.000**	0.180
kNDVI-Sunny	kNDVI-Shade	0.655	0.025	0.655	0.371

attributed to the gradual process of chlorophyll degradation during defoliation—encompassing leaf nutrient relocation, chlorophyll breakdown, leaf coloration, and shedding (Mariën et al., 2019). These processes are highly influenced by climate fluctuations, resulting in weaker and slower spectral signal changes. In contrast, spring leaf flushing, occurring after a leafless period, is characterized by rapid leaf greening, leading to more distinct spectral changes.

Our findings indicated that kNDVI demonstrated higher accuracy in extracting rubber leaf fall phenology compared to NDVI, EVI and NIRv (Fig. 4). Wang et al. (2023c) demonstrated that kNDVI exhibited the strongest correlation with biophysical parameters and GPP, followed by NIRv and NDVI. The kNDVI outweighs NDVI and NIRv by addressing saturation issues in regions with high vegetation cover, which improves the accuracy of defoliation phenology extraction. Furthermore, NIRv exhibits low RMSE in extracting rubber refoliation phenology in this study. This finding aligns with the results of Zhang et al. (2022) and Ersi et al. (2022), who found that SIF and NIRv are more effective at capturing detailed vegetation dynamics than NDVI and EVI. During leaf flushing, new rubber leaves exhibit strong photosynthetic activity, leading to rapidly increased chlorophyll absorption of red light (R) and a significant rise in NIR reflectance. This makes NIRv, the product of NDVI and NIR, more sensitive and more effective in capturing the phenological status of refoliation in rubber plantations (Zeng et al., 2020). In the future, kNDVI and NIRv indices should be further explored for phenological extraction in rubber plantations or other types of tropical vegetation across different regions.

This study found that the SOD of rubber plantations in Xishuangbanna primarily occurred in January, with the leaf fall period typically ending between January 16 and mid-February (Fig. 5). These findings are consistent with previous studies conducted in Yunnan Province, China (Liyanage et al., 2019; Zhai et al., 2019), which reported that the SOD mainly occurred from late December to January. We also found a significant delayed trend of SOD from 2003 to 2022 (Fig. 7 and Table 3), which aligns with the majority of studies reporting delayed trends in temperate forests (Menzel et al., 2006; Liu et al., 2016). The delayed trend in rubber plantations (0.14 days/year) was comparable to the observed delay in most temperate deciduous forests (0.16 ± 0.01 days/year). The delay was primarily attributed to the increased temperatures due to global warming (Piao et al., 2019; Azizan et al., 2023). For instance, Shi et al. (2014) proposed that the primary mechanism behind delayed leaf fall was the increased activity of photosynthetic enzymes and slower chlorophyll degradation during leaf senescence, caused by the rising temperature. Globally, extensive studies have reported the advanced SOR with both in-situ observations and satellites across North America, Europe, and Easten Asia (Chmielewski et al., 2001; Wolfe et al., 2005; Richardson et al., 2013; Ge et al., 2014). However, the amplitude of this advancement varied due to differences in

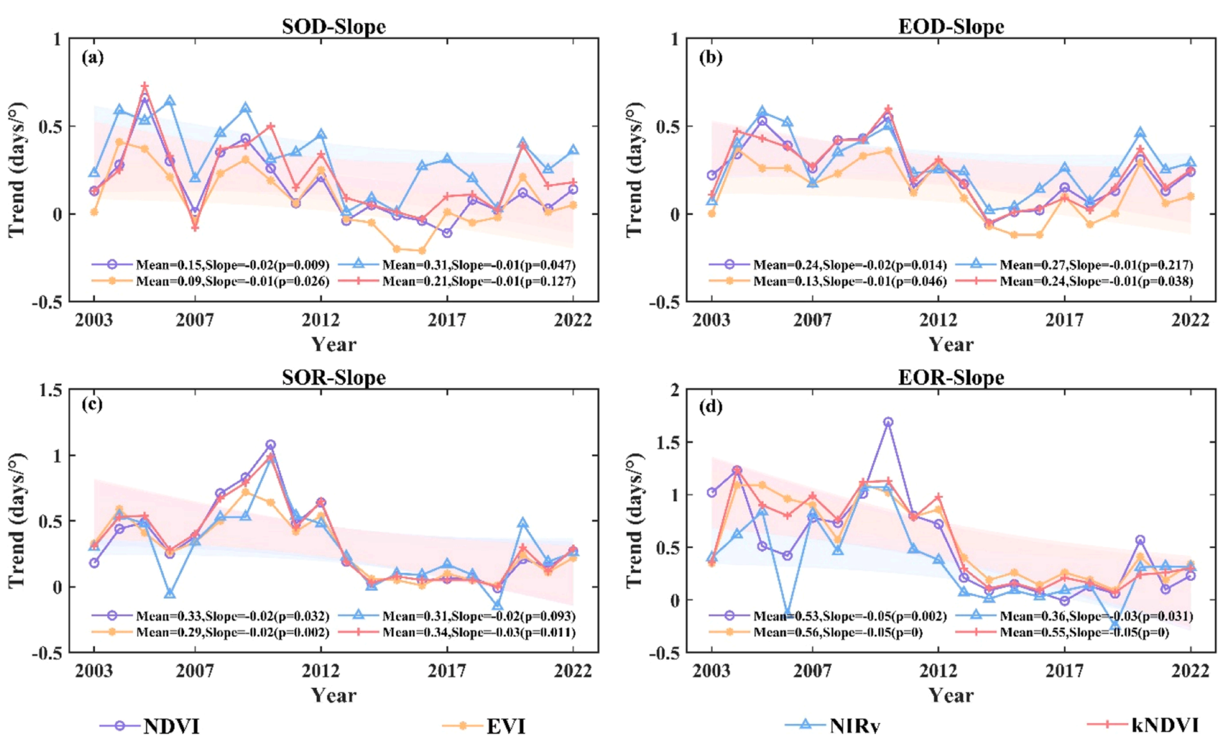

Fig. 9. Rubber phenology trend at different slope.

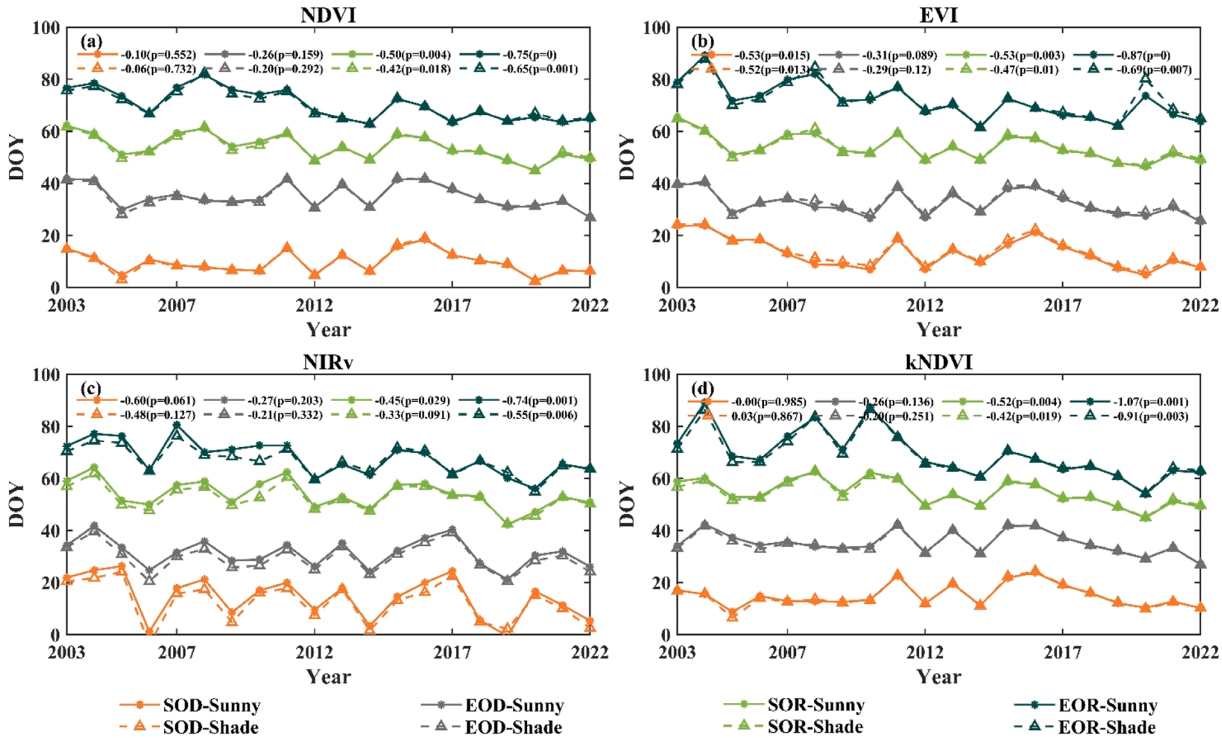

Fig. 10. Comparison of rubber phenology metrics at different aspects.

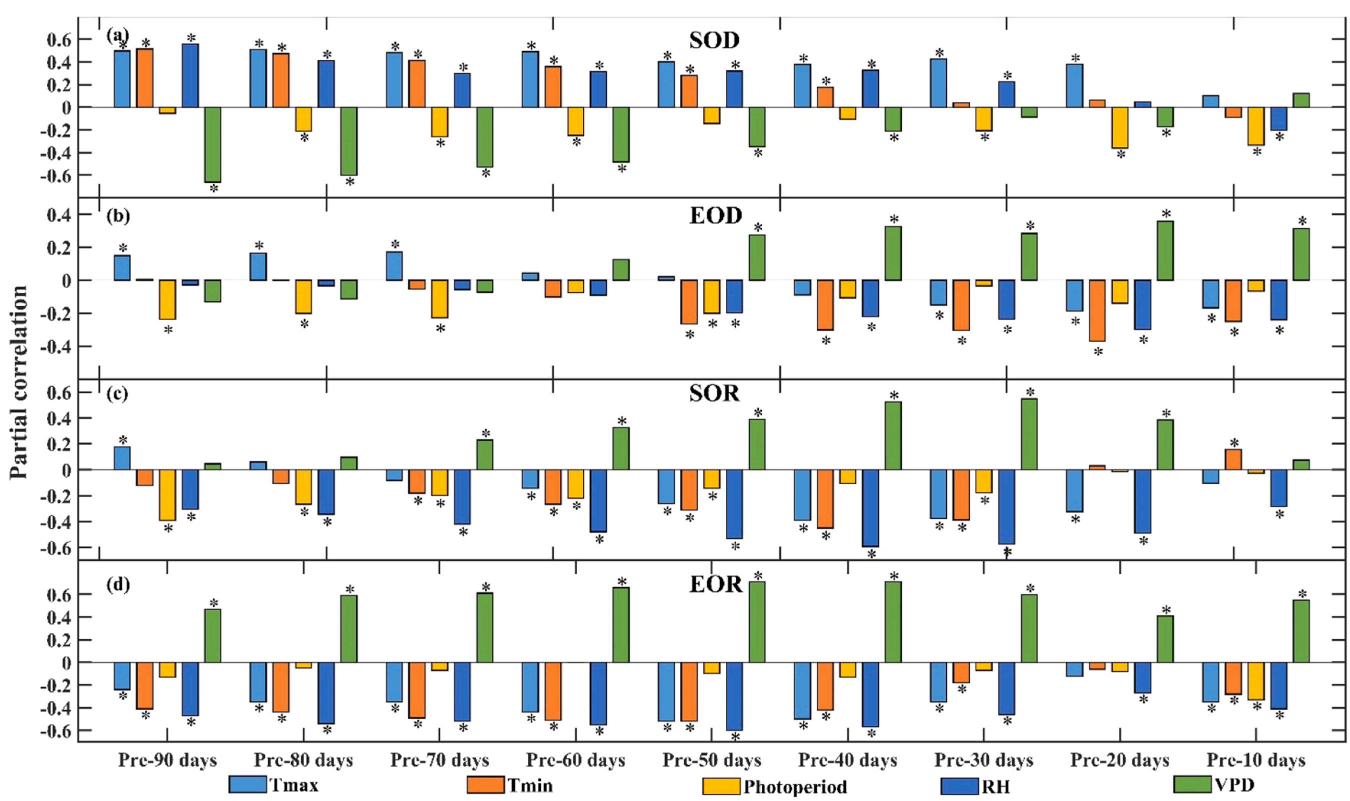

Fig. 11. Partial correlation coefficients between four phenology dates ((a) SOD, (b) EOD, (c) SOR and (d) EOR) and climate factors. * represents significance at α= 0.05.

the studied regions, periods, and tree species. (Piao et al., 2019). Similarly, in this study, the SOR and EOR of rubber plantations also exhibited significant advanced trends from 2003 to 2022, with rates of 0.34 days/year, and 0.66 days/year, respectively.

Existing previous studies have revealed significant regional differences of rubber phenology (Liu et al., 2013; Yang et al., 2019). Dong et al. (2013) found that the SOD and EOD primarily occurred from late February to late March, while the SOR and EOR mainly occurred from

Table 5
Quantified influences of driving factors on rubber phenological using the PLS-PM model.

Phenology metrics	Pre-days	Path coefficients		Temperature loading		Humidity loading	
		Temp	Humidity	Tmin	Tmax	VPD	RH
SOD	90	0.52	**−0.86**	**0.81**	0.62	**0.99**	0.26
	80	0.43	**−0.60**	0.46	**0.91**	**0.95**	0.02
	70	0.13	**−0.20**	**0.97**	−0.14	**0.68**	−0.59
	60	**0.52**	−0.45	0.64	**0.80**	0.46	**−0.85**
	50	**0.54**	−0.30	0.66	**0.86**	**1.00**	−0.03
	40	**0.69**	−0.27	0.61	**0.92**	**0.98**	−0.17
	30	**0.68**	−0.18	0.59	**0.90**	**0.96**	−0.25
	20	**0.43**	−0.19	0.71	**0.88**	**0.90**	−0.60
	10	**0.28**	−0.06	**1.00**	0.39	**0.98**	−0.46
EOD	90	0.002	**−0.12**	**0.88**	0.59	**0.91**	0.70
	80	0.001	**−0.11**	**0.91**	−0.31	0.74	**0.84**
	70	0.02	**−0.11**	−0.04	**0.98**	0.05	**0.99**
	60	0.01	**−0.15**	0.29	**1.00**	−0.41	**0.85**
	50	−0.15	**−0.35**	0.63	**0.93**	**−0.78**	0.51
	40	−0.12	**−0.29**	0.49	**0.94**	−0.70	**0.73**
	30	−0.21	**−0.34**	0.66	**0.89**	−0.72	**0.80**
	20	−0.06	**−0.21**	**0.96**	0.29	−0.72	**0.74**
	10	−0.19	**−0.34**	0.42	**0.88**	−0.68	**0.78**
SOR	90	0.003	**−0.32**	0.05	**1.00**	0.29	**0.99**
	80	−0.09	**−0.40**	0.29	**0.98**	0.11	**0.97**
	70	−0.13	**−0.46**	0.62	**0.85**	−0.19	**0.90**
	60	−0.11	**−0.48**	**0.91**	0.47	−0.52	**0.71**
	50	0.33	**−0.44**	**0.74**	−0.68	−0.42	**0.85**
	40	**0.46**	−0.42	0.66	**−0.75**	−0.59	**0.77**
	30	**0.36**	−0.25	**0.81**	−0.71	**0.94**	−0.33
	20	**0.24**	0.18	**0.95**	−0.53	**1.00**	0.02
	10	**0.23**	0.07	**0.99**	−0.39	**1.00**	0.16
EOR	90	**−0.38**	0.20	0.32	**0.84**	**0.80**	−0.74
	80	**−0.17**	0.06	0.39	**0.79**	0.41	**−0.96**
	70	−0.56	**0.56**	**0.66**	0.49	**0.98**	−0.33
	60	−0.07	**0.27**	−0.53	**0.98**	**0.91**	−0.52
	50	−0.50	**0.80**	0.03	**0.95**	**0.94**	−0.45
	40	−0.54	**0.97**	−0.11	**0.97**	**0.82**	−0.64
	30	−0.26	**0.90**	0.12	**0.89**	**0.94**	−0.35
	20	−0.09	**0.80**	0.41	**0.77**	**0.98**	−0.12
	10	−0.08	**0.72**	**0.92**	0.14	**0.98**	0.38

late March to April in Danzhou, Hainan Province, China. This indicates that the four rubber phenologies in Hainan Province occurred later than those in Xishuangbanna reported by this study. Chen et al. (2022) also found large variation of defoliation durations among different latitudes (An increase of one degree in latitude decreases the defoliation duration by 2.9 days, R^2=0.96) and suggested that the possible reason for these regional differences was the reaching time variation of low-temperature threshold during the dry season across different locations. Besides, other factors, such as water availability and management practices, may also contribute the regional differences. For example, Chen et al. (2010) and Liu et al. (2014) suggested that drought stress was the main cause of rubber defoliation phenology. The control effectiveness of rubber leaf powdery mildew affects the growth of new leaves, thereby influencing leaf flushing phenology (Liyanage et al., 2019; Zhai et al., 2023).

Our study found topography significantly affects the rubber phenology. The four phenological dates generally showed delayed trend with both increasing elevation and slope. The SOD, EOD, SOR, and EOR based on the four VIs were averagely delayed by 0.27 days/50 m, 0.44 days/50 m, 0.72 days/50 m, and 0.91 days/50 m, respectively. Guyon et al. (2011) reported that the SOR of deciduous broad-leaved forests in France was delayed by an average of 2.3 days for every 100-meter increase in elevation. The possible reasons for the delayed phenology vary. Lower temperature due to increased elevation may be the major reason leading to delayed SOR and EOR (Liyanage et al., 2019; Azizan et al., 2021). For the delayed SOD, the most possible reason may be the increased humidity due to increased elevation (Carr, 2012; Guerra-Hincapié et al., 2020). Our results show that the SOD, EOD, SOR, and EOR based on the four VIs were averagely delayed by 0.19 days/°, 0.22 days/°, 0.32 days/°, and 0.50 days/°, respectively. Few studies have examined the impact of slope on phenology. This is probably due to the complex effects of slope on microclimate. We suggested the delayed rubber phenology of increased slope is a comprehensive result of changed temperature and humidity.

4.2. Response of rubber phenology to meteorology

Causes of rubber leaf fall have been a topic of debate over the past several decades. For instance, Lin et al. (2018) and Chen et al. (2022) found that cold stress correlated more closely with defoliation metrics than drought stress in Xishuangbanna, suggesting that low-temperature stress might be the driving factor. Conversely, Liu et al. (2014) and Chen et al. (2010) addressed drought dress and suggested that leaves began to senesce due to the low water conductivity in the xylem vessels (the plant structures responsible for water transport). Guerra-Hincapié et al. (2020) argued that in rubber plantations, rainfall was the most critical climatic factor inducing leaf fall.Guardiola-Claramonte et al. (2010) found that rubber defoliation was caused by a combination of factors rather than a single one, including water availability, temperature, and daylength. Our analysis also revealed that both temperature and humidity jointly determined the timing of SOD, with temperature being more influential than humidity. Our findings may be more reasonable as the following reasons: low temperatures can cause cell damage and metabolic disorders in leavesthrough mechanisms such as enzyme activity, membrane integrity, and oxidative stress, stimulating rubber trees to reallocate nutrients from mature leaves to the trunk as an adaptive response during the leaf senescence period (Waraich et al., 2012;

Hasanuzzaman et al., 2013; Li et al., 2016). Additionally, by shedding leaves, rubber trees reduce transpiration in dry season and consequently alleviate the stress caused by decreased soil moisture (Kobayashi et al., 2014; Wang et al., 2023b). This dual strategy helps the trees manage both low-temperature stress and water scarcity effectively.

In contrast to the debated causes of SOD, there is a general agreement among scholars on the primary drivers of SOR on most deciduous forests (i.e., temperature) (Fu et al., 2015; Picornell et al., 2019; Azizan et al., 2023). Our results indicated the SOR of rubber plantations was jointly influenced by temperature and humidity, with both factors showing a negative correlation. This finding is consistent with the analysis of the driving mechanisms conducted by Lai et al. (2023). We also found the impact of humidity on SOR was stronger than that of temperature. This is reasonable as SOR primarily occurs in the latter part of the dry season. During this period, temperature variations are relatively small, whereas humidity increases significantly, providing sufficient water for leaf bud development. Humidity regulates leaf unfolding by influencing water balance and cell turgor. High humidity facilitates water replenishment through root water absorption and further facilitates leaf transpiration and photosynthesis, while low humidity may inhibits leaf growth and unfolding by reducing stomatal aperture (Farooq et al., 2009; Kaur et al., 2021). Compared to SOD and SOR, the driving factors for EOD and EOR are poorly understood, particularly for rubber plantations. In this study, we found that increased humidity accelerated EOR, indicating that humidity plays a dominant role in the spring phenonogy (Farooq et al., 2009; Waraich et al., 2012; Hasanuzzaman et al., 2013; Kaur et al., 2021). Although RH is found to be the primary climatic factor influencing EOD, the role of RH on EOD might not be decisive as its climatic correlation with EOD is less than 0.4 and its path coefficient is also relatively small. This also implied that the drivers of EOD are much more complex than the other three phenological dates.

4.3. Uncertainty and future direction

One of the primary challenges in rubber phenology monitoring is the data contamination caused by tropical cloudy and rainy weather (Guyon et al., 2011; Shen et al., 2024). The coarser resolution of quality control bands may result in undetected sub-pixel clouds and landscape shadows, contributing to data contamination and ultimately leading to the uncertainty of rubber phenology monitoring. Mixed pixels can also introduce errors. For instance, although the resampled 250-meter pixel contains over 90 % of the 30-meter rubber plantation pixels, the remaining 10 % non-rubber pixels may still bring uncertainties in the calculation of VIs. The second uncertainty may come from the topographic effects on reflectance. Since rubber plantations are primarily located in mountainous regions in Xishuangbanna, reflectance errors caused by topographic effects can influence phenology monitoring. However, we suggest this influence would be partially eliminated by the calculation of vegetation indices, especially for the ratio indices such as NDVI. In terms of method, we attempted to use the commonly employed method of interpolation with adjacent dates, but found that the increased gap-filling rate was still insufficient to construct an integrated daily-scale time series curve. Therefore, we further complemented the missing pixels based on homogeneous pixels with the same planting characteristics and elevation, reducing the data gap rate to less than 30 %. However, even if a daily time series can be constructed, spectral differences between interpolated pixels and actual pixels still exist (Atkinson et al., 2012; Bolton et al., 2020), leading to errors in extracting phenological metrics. The VI time series were reconstructed through smoothing and fitting to extract phenological metrics. This process may attenuate sudden VI changes due to extreme climatic events, potentially causing shifts in phenological extraction dates and impacting the overall phenological trend. Finally, uncertainty may also come from the inconsistency between ground-based phenological observations and satellite-derived phenological estimates. Satellite-derived phenology is primarily estimated based on changes in vegetation reflectance, whereas ground-based phenology is defined according to biological theories related to leaf development levels (Hmimina et al., 2013), leading to fundamentally different mechanisms. Additionally, due to spatiotemporal heterogeneity of individual trees, validating satellite-derived phenology at the pixel scale (ranging from tens of meters to kilometers) against ground-based observations from a few trees involves significant uncertainties (Shen et al., 2024). The latest advancements in near-surface remote sensing methods, such as PhenoCams (Tools for monitoring plant phenological changes) and drones, offer the potential to bridge ground-based and satellite-derived phenology (Richardson et al., 2018; Li et al., 2021).

In the future, firstly, determining thresholds for vegetation time series corresponding to each phenological event requires standardization. Currently, there is no unified and widely accepted threshold for rubber phenology. Azizan et al. (2021) applied 20 % seasonal amplitude threshold to extract the EOD and SOR of rubber in Indonesia. Meanwhile, Lai et al. (2023) determined 15 % and 20 % to extract EOD and SOR of rubber in Yunnan province, China. Hu et al. (2022) set 60 % and 30 % to extract SOD and SOR of rubber in Hainan province, China. To minimize uncertainty from subjective threshold setting, this study extracted rubber phenology by comparing different thresholds and validating the optimal one using PhenoCam imagery. Our results show that 20 % and 5 % thresholds are optimal for extracting the start of defoliation and refoliation in rubber plantations using the four indices. However, further studies should be conducted to assess their reliability and applicability in other regions or ecosystems.

Secondly, to better monitor rubber phenology, future efforts should focus on using multi-source remote sensed imagery to improve spatiotemporal resolution. This can be achieved by integrating high temporal resolution data (e.g., MODIS) with medium-high spatial resolution data (e.g., Landsat, Sentinel-2) using mature fusion algorithms such as the Enhanced Spatial and Temporal Adaptive Reflectance Fusion Model (ESTARFM) (White et al., 2009; Zeng et al., 2020). Additionally, Synthetic Aperture Radar (SAR) can penetrate cloud cover to obtain canopy structure information, as it is minimally affected by clouds and rain, making it a valuable tool for monitoring vegetation phenology in cloudy regions. However, SAR may encounter challenges in high-density vegetation areas, where dense canopies can attenuate the radar signal, reducing accuracy in estimating vegetation structure and biomass. Recent studies have also found that Solar-Induced Chlorophyll Fluorescence (SIF) can directly measure photosynthetic activity, showing higher sensitivity to vegetation greenness changes and being less affected by clouds and atmospheric scattering (Mohammed et al., 2019; Xu et al., 2023). This provides new possibilities for monitoring rubber phenology. However, the coarse spatial resolution of current SIF data (e.g., 0.05° for GOSIF) may be insufficient for accurately monitoring rubber plantations, particularly in heterogeneous landscapes or small-scale plantations. Therefore, effectively combining different data sources for phenological extraction remains an area for further exploration. However, there are still many challenges and limitations in the fusion of these data, which mainly manifest in the following aspects: (1) Due to the differing geometric accuracies of the various datasets, fusion of different data sources may introduce new registration errors. This can result in spectral signal distortion, which, in turn, affects phenological assessment (Ghamisi et al., 2019); (2) The spectral response ranges of different optical data are inconsistent, so the fusion process is prone to spectral distortion, which affects the extraction of phenological information (Ghassemian, 2016); (3) The structural differences between SAR and optical data are even greater, making signal distortion more likely during the fusion process (Kulkarni et al., 2020). Thus, the improvements in fusion algorithms in future may provide great potential in monitoring phenology of tropical plantations.

Lastly, major rubber-producing countries should actively establish phenological and meteorological observation systems with standardized observation protocols. Currently, most countries have relatively short historical records and limited stable and consistent monitoring locations for vegetation phenology except for some developed countries such as Germany, Finland, Sweden, and Japan (Morellato et al., 2013; Peng et al., 2017). For rubber plantation, besides China and Thailand, which have a few monitoring sites, there are no reports from other countries in the Lancang-Mekong region. Establishing a standardized phenological and meteorological observation network in Southeast Asian countries would enhance our understanding of the mechanisms driving rubber plantation phenology.

5. Conclusions

The study of phenology monitoring and its driving mechanisms in rubber plantations can help improve plantation management and optimize tapping schedules. In this study, we investigated the performance of four vegetation indices in monitoring rubber phenology metrics. In addition, we also investigated their spatiotemporal patterns and responses to climate dynamics and topography. The results showed that kNDVI performed best in monitoring defoliation metrics (SOD and EOD) while NIRv outweighed in extracting refoliation metrics (SOR and EOR). EOD, SOR and EOR showed averagely advanced trend with 0.13, 0.34, and 0.66 days per year, respectively, while SOD showed no significant trend from 2003 to 2022. All four phenological dates generally showed a delayed trend with increasing elevation and slope. Partial correlation and path analysis suggested that temperature variables (Tmax and Tmin) and humidity variables (RH and VPD) jointly regulated the SOD and EOD, whereas humidity variables predominantly influenced SOR and EOR. This study fills the knowledge gap on the spatiotemporal trends of four rubber phenology events and their response to climatic and topographic factors, and help a better understanding of phenology in tropical tree species. Future efforts should focus on integrating multi-source remote sensing data (e.g., microwave imagery, SIF data, etc.) to improve the retrieval accuracy of rubber phenology and constructing a phenological and meteorological observation network in major rubber-producing countries to better investigate the response of rubber phenology to future climate change.

CRediT authorship contribution statement

Lu Dengsheng: Supervision, Methodology. **Wang Shusen:** Supervision, Methodology. **Chen Yanling:** Writing – original draft, Visualization, Validation, Software, Methodology, Investigation, Formal analysis, Conceptualization. **Khongdee Nuttapaon:** Writing – original draft, Methodology, Investigation. **Wang Yaofeng:** Writing – original draft, Methodology, Investigation. **Song Qinghai:** Supervision, Methodology. **Chen Yaoliang:** Writing – review & editing, Writing – original draft, Supervision, Resources, Methodology, Investigation, Funding acquisition, Formal analysis, Conceptualization.

Declaration of Competing Interest

The authors declare that they have no known competing financial interests or personal relationships that could have appeared to influence the work reported in this paper.

Acknowledgments

This work was supported by the National Natural Science Foundation of China (grant number 42277450) and the Open Fund from the CAS Key Laboratory of Tropical Forest Ecology (grant number 20-CAS-TFE-01). We thank the Xishuangbanna Tropical Botanical Garden of Chinese Academy of Sciences for providing climate and phenology observation data.

Data availability

Data will be made available on request.

References

Ahrends, A., Hollingsworth, P.M., Ziegler, A.D., Fox, J.M., Chen, H.F., Su, Y.F., Xu, J.C., 2015. Current trends of rubber plantation expansion may threaten biodiversity and livelihoods. Glob. Environ. Change 34, 48–58. https://doi.org/10.1016/j.gloenvcha.2015.06.002.

Atkinson, P.M., Jeganathan, C., Dash, J., Atzberger, C., 2012. Inter-comparison of four models for smoothing satellite sensor time-series data to estimate vegetation phenology. Remote Sens. Environ. 123, 400–417. https://doi.org/10.1016/j.rse.2012.04.001.

Azizan, F.A., Astuti, I.S., Aditya, M.I., Febbiyanti, T.R., Williams, A., Young, A., Abdul Aziz, A., 2021. Using multi-temporal satellite data to analyse phenological responses of rubber (Hevea brasiliensis) to Climatic Variations in South Sumatra, Indonesia. Remote Sens 13 (15), 2932. https://doi.org/10.3390/rs13152932.

Azizan, F., Astuti, I., Young, A., Aziz, A.A., 2023. Rubber leaf fall phenomenon linked to increased temperature. Agric. Ecosyst. Environ. 352, 108531. https://doi.org/10.1016/j.agee.2023.108531.

Badgley, G., Field, C.B., Berry, J.A., 2017. Canopy near-infrared reflectance and terrestrial photosynthesis. Sci. Adv. 3 (3), e1602244. https://doi.org/10.1126/sciadv.1602244.

Berra, E.F., Gaulton, R., 2021. Remote sensing of temperate and boreal forest phenology: a review of progress, challenges and opportunities in the intercomparison of in-situ and satellite phenological metrics. For. Ecol. Manag. 480, 118663. https://doi.org/10.1016/j.foreco.2020.118663.

Bolton, D.K., Gray, J.M., Melaas, E.K., Moon, M., Eklundh, L., Friedl, M.A., 2020. Continental-scale land surface phenology from harmonized Landsat 8 and Sentinel-2 imagery. Remote Sens. Environ. 240, 111685. https://doi.org/10.1016/j.rse.2020.111685.

Camps-Valls, G., Campos-Taberner, M., Moreno-Martínez, Á., Walther, S., Duveiller, G., Cescatti, A., Mahecha, M.D., Muñoz-Marí, J., García-Haro, F.J., Guanter, L., 2021. A unified vegetation index for quantifying the terrestrial biosphere. Sci. Adv. 7 (9), eabc7447. https://doi.org/10.1126/sciadv.abc7447.

Carr, M., 2012. The water relations of rubber (Hevea brasiliensis): a review. Exp. Agric. 48 (2), 176–193. https://doi.org/10.1017/S0014479711000901.

Chen, J.W., Cao, K.F., 2015. A possible link between hydraulic properties and leaf habits in Hevea brasiliensis. Funct. Plant Biol. 42 (8), 718–726. https://doi.org/10.1071/FP14294.

Chen, Y.L., Wang, S.S., Zhou, R.W., Gnanamoorthy, P., Song, Q.H., Chen, H.B., 2022. What leads to rubber leaf senescence in the northern edge of the Asian tropics. Ind. Crops Prod. 178, 114617. https://doi.org/10.1016/j.indcrop.2022.114617.

Chen, J.W., Zhang, Q., Li, X.S., Cao, K.F., 2010. Gas exchange and hydraulics in seedlings of Hevea brasiliensis during water stress and recovery. Tree Physiol. 30 (7), 876–885. https://doi.org/10.1093/treephys/tpq043.

Chmielewski, F.-M., Rötzer, T., 2001. Response of tree phenology to climate change across Europe. Agric. For. Meteorol. 108 (2), 101–112. https://doi.org/10.1016/S0168-1923(01)00233-7.

Cui, L.L., Shi, J., Du, H.Q., 2021. Advances in remote sensing extraction of vegetation phenology and its driving factors. Adv. Earth Sci. 36 (01), 9–16. https://doi.org/10.11867/j.issn.1001-8166.2021.006.

Dong, J.W., Xiao, X.M., Chen, B.Q., Torbick, N., Jin, C., Zhang, G.L., Biradar, C., 2013. Mapping deciduous rubber plantations through integration of PALSAR and multi-temporal Landsat imagery. Remote Sens. Environ. 134, 392–402. https://doi.org/10.1016/j.rse.2013.03.014.

Ersi, C., Bayaer, T., Bao, Y., Bao, Y., Yong, M., Lai, Q., Zhang, X., Zhang, Y., 2022. Comparison of phenological parameters extracted from SIF, NDVI and NIRv data on the Mongolian plateau. Remote Sens 15 (1), 187. https://doi.org/10.3390/rs15010187.

Farooq, M., Wahid, A., Kobayashi, N., Fujita, D., Basra, S.M., 2009. Plant drought stress: effects, mechanisms and management. Sustain. Agric. 153–188. https://doi.org/10.1051/agro:2008021.

Fu, Y.S., Zhao, H.F., Piao, S.L., Peaucelle, M., Peng, S.S., Zhou, G.Y., Ciais, P., Huang, M. T., Menzel, A., Peñuelas, J., 2015. Declining global warming effects on the phenology of spring leaf unfolding. Nature 526 (7571), 104–107. https://doi.org/10.1038/nature15402.

Ge, Q.S., Wang, H.J., Rutishauser, T., Dai, J.H., 2014. Phenological response to climate change in China: a meta-analysis. Glob. Change Biol. 21 (1), 265–274. https://doi.org/10.1111/gcb.12648.

George, S., Suresh, P., Wahid, P., Nair, R.B., Punnoose, K., 2009. Active root distribution pattern of Hevea brasiliensis determined by radioassay of latex serum. Agrofor. Syst. 76, 275–281. https://doi.org/10.1007/s10457-008-9104-y.

Ghamisi, P., Rasti, B., Yokoya, N., Wang, Q., Hofle, B., Bruzzone, L., Bovolo, F., Chi, M., Anders, K., Gloaguen, R., 2019. Multisource and multitemporal data fusion in remote sensing: a comprehensive review of the state of the art. IEEE Trans. Geosci. Remote Sens. 7 (1), 6–39. https://doi.org/10.1109/MGRS.2018.2890023.

Ghassemian, H., 2016. A review of remote sensing image fusion methods. Inf. Fusion. 32, 75–89. https://doi.org/10.1016/j.inffus.2016.03.003.

Guardiola-Claramonte, M., Troch, P.A., Ziegler, A.D., Giambelluca, T.W., Durcik, M., Vogler, J.B., Nullet, M.A., 2010. Hydrologic effects of the expansion of rubber (Hevea brasiliensis) in a tropical catchment. Ecohydrology 3 (3), 306–314. https://doi.org/10.1002/eco.110.

Guerra-Hincapié, J.J., Córdoba-Gaona, O. d J., Gil-Restrepo, J.P., Monsalve-García, D.A., Hernández-Arredondo, J.D., Martínez-Bustamante, E.G., 2020. Phenological patterns of defoliation and refoliation processes of rubber tree clones in the colombian northwest. Rev. Fac. Nac. De. Agron. Medellin 73 (3), 9293–9303. https://doi.org/10.15446/rfnam.v73n3.80546.

Gutiérrez-Vanegas, A.J., Correa-Pinilla, D.E., Gil-Restrepo, J.P., López-Hernández, F.G., Guerra-Hincapié, J.J. and Córdoba-Gaona, O. d J., 2020. Foliar and flowering phenology of three rubber (Hevea brasiliensis) clones in the eastern plains of Colombia. Brazilian Journal of Botany. 43 (4), 813-821.

Guyon, D., Guillot, M., Vitasse, Y., Cardot, H., Hagolle, O., Delzon, S., Wigneron, J.-P., 2011. Monitoring elevation variations in leaf phenology of deciduous broadleaf forests from SPOT/VEGETATION time-series. Remote Sens. Environ. 115 (2), 615–627. https://doi.org/10.1016/J.RSE.2010.10.006.

Hasanuzzaman, M., Nahar, K., Fujita, M., 2013. Extreme temperature responses, oxidative stress and antioxidant defense in plants. Abiotic Stress-Plant Responses Appl. Agric. 13, 169–205.

Hmimina, G., Dufrêne, E., Pontailler, J.-Y., Delpierre, N., Aubinet, M., Caquet, B., De Grandcourt, A., Burban, B., Flechard, C., Granier, A., 2013. Evaluation of the potential of MODIS satellite data to predict vegetation phenology in different biomes: an investigation using ground-based NDVI measurements. Remote Sens. Environ. 132, 145–158. https://doi.org/10.1016/j.rse.2013.01.010.

Hu, Y.Y., Dai, S.P., Luo, H.X., Li, H.L., Li, M.F., Zheng, Q., Yu, X., Li, N., 2022. Spatio-temporal change characteristics of rubber forest phenology in Hainan Island during 2001—2015. Remote Sens. Nat. Resour. 34 (1), 210–217. https://doi.org/10.6046/zrzyyg.2021110.

Jeong, S.-J., Schimel, D., Frankenberg, C., Drewry, D.T., Fisher, J.B., Verma, M., Berry, J. A., Lee, J.-E., Joiner, J., 2017. Application of satellite solar-induced chlorophyll fluorescence to understanding large-scale variations in vegetation phenology and function over northern high latitude forests. Remote Sens. Environ. 190, 178–187. https://doi.org/10.1016/j.rse.2016.11.021.

Jonsson, P., Eklundh, L., 2002. Seasonality extraction by function fitting to time-series of satellite sensor data. IEEE Trans. Geosci. Remote Sens. 40 (8), 1824–1832. https://doi.org/10.1109/TGRS.2002.802519.

Jönsson, P., Eklundh, L., 2004. TIMESAT—a program for analyzing time-series of satellite sensor data. Comput. Geosci. 30 (8), 833–845. https://doi.org/10.1016/j.cageo.2004.05.006.

Kaur, H., Kohli, S.K., Khanna, K., Bhardwaj, R., 2021. Scrutinizing the impact of water deficit in plants: transcriptional regulation, signaling, photosynthetic efficacy, and management. Physiol. Plant. 172 (2), 935–962. https://doi.org/10.1111/ppl.13389.

Kobayashi, N., Kumagai, T. o, Miyazawa, Y., Matsumoto, K., Tateishi, M., Lim, T.K., Mudd, R.G., Ziegler, A.D., Giambelluca, T.W., Yin, S., 2014. Transpiration characteristics of a rubber plantation in central Cambodia. Tree Physiol. 34 (3), 285–301. https://doi.org/10.1093/treephys/tpu009.

Kulkarni, S.C., Rege, P.P., 2020. Pixel level fusion techniques for SAR and optical images: a review. Inf. Fusion. 59, 13–29. https://doi.org/10.1016/j.inffus.2020.01.003.

Lai, H.Y., Chen, B.Q., Yin, X., Wang, G.Z., Wang, X.C., Yun, T., Lan, G.Y., Wu, Z.X., Yang, C., Kou, W.L., 2023. Dry season temperature and rainy season precipitation significantly affect the spatio-temporal pattern of rubber plantation phenology in Yunnan province. Front. Plant Sci. 14, 1283315. https://doi.org/10.3389/fpls.2023.1283315.

Li, Y.W., Lan, G.Y., Xia, Y.J., 2016. Rubber trees demonstrate a clear retranslocation under seasonal drought and cold stresses. Front. Plant Sci. 7, 234645. https://doi.org/10.3389/fpls.2016.01907.

Li, Q., Shen, M.G., Chen, X.H., Wang, C., Chen, J., Cao, X., Cui, X.H., 2021. Optimal color composition method for generating high-quality daily photographic time series from PhenoCam. IEEE J. Sel. Top. Appl. Earth Obs. Remote Sens. 14, 6179–6193. https://doi.org/10.1109/JSTARS.2021.3087814.

Li, H., Zhao, J.Y., 2018. Evaluation of the newly released worldwide AW3D30 DEM over typical landforms of China using two global DEMs and ICESat/GLAS data. IEEE J. Sel. Top. Appl. Earth Obs. Remote Sens. 11 (11), 4430–4440. https://doi.org/10.1109/JSTARS.2018.2874361.

Lin, Y.X., Zhang, Y.P., Zhao, W., Dong, Y.X., Fei, X.H., Song, Q.H., Sha, L.Q., Wang, S.S., Grace, J., 2018. Pattern and driving factor of intense defoliation of rubber plantations in SW China. Ecol. Indic. 94, 104–116. https://doi.org/10.1016/j.ecolind.2018.06.050.

Liu, X.N., Feng, Z.M., Jiang, L.G., Li, P., Liao, C.H., Yang, Y.Z., You, Z., 2013. Rubber plantation and its relationship with topographical factors in the border region of China, Laos and Myanmar. J. Geogr. Sci. 23, 1019–1040. https://doi.org/10.1007/s11442-013-1060-4.

Liu, Q., Fu, Y.S., Zeng, Z.Z., Huang, M.T., Li, X.R., Piao, S.L., 2016. Temperature, precipitation, and insolation effects on autumn vegetation phenology in temperate China. Glob. Change Biol. 22 (2), 644–655. https://doi.org/10.1111/gcb.13081.

Liu, W.J., Li, J.T., Lu, H.J., Wang, P.Y., Luo, Q.P., Liu, W.Y., Li, H.M., 2014. Vertical patterns of soil water acquisition by non-native rubber trees (Hevea brasiliensis) in Xishuangbanna, southwest China. Ecohydrology 7 (4), 1234–1244. https://doi.org/10.1002/eco.1456.

Liyanage, K., Khan, S., Ranjitkar, S., Yu, H., Xu, J., Brooks, S., Beckschäfer, P., Hyde, K. D., 2019. Evaluation of key meteorological determinants of wintering and flowering patterns of five rubber clones in Xishuangbanna, Yunnan, China. Int. J. Biometeorol. 63, 617–625. https://doi.org/10.1007/s00484-018-1598-z.

Mann, H.B., 1945. Nonparametric tests against trend. Econometrica 245–259. https://doi.org/10.2307/1907187.

Mariën, B., Balzarolo, M., Dox, I., Leys, S., Lorène, M.J., Geron, C., Portillo-Estrada, M., AbdElgawad, H., Asard, H., Campioli, M., 2019. Detecting the onset of autumn leaf senescence in deciduous forest trees of the temperate zone. N. Phytol. 224 (1), 166–176. https://doi.org/10.1111/nph.15991.

McIntosh, C.N., Edwards, J.R., Antonakis, J., 2014. Reflections on partial least squares path modeling. Organ. Res. Methods 17 (2), 210–251. https://doi.org/10.1177/1094428114529165.

Melaas, E.K., Friedl, M.A., Zhu, Z., 2013. Detecting interannual variation in deciduous broadleaf forest phenology using Landsat TM/ETM+ data. Remote Sens. Environ. 132, 176–185. https://doi.org/10.1016/j.rse.2013.01.011.

Menzel, A., Sparks, T.H., Estrella, N., Koch, E., Aasa, A., Ahas, R., Alm-Kübler, K., Bissolli, P., Braslavská, O. g, Briede, A., 2006. European phenological response to climate change matches the warming pattern. Glob. Change Biol. 12 (10), 1969–1976. https://doi.org/10.1111/j.1365-2486.2006.01193.x.

Mohammed, G.H., Colombo, R., Middleton, E.M., Rascher, U., van der Tol, C., Nedbal, L., Goulas, Y., Pérez-Priego, O., Damm, A., Meroni, M., 2019. Remote sensing of solar-induced chlorophyll fluorescence (SIF) in vegetation: 50 years of progress. Remote Sens. Environ. 231, 111177. https://doi.org/10.1016/j.rse.2019.04.030.

Morellato, L.P.C., Camargo, M.G.G., Gressler, E., 2013. A review of plant phenology in South and Central America. Phenol.: Integr. Environ. Sci. 91–113. https://doi.org/10.1007/978-94-007-6925-0_6.

National Bureau of Statistics of China, 2023. Xishuangbanna Statistics Yearbook 2022. Xishuangbanna. China Statistics Press, p. 59.

Peng, D.L., Wu, C.Y., Li, C.J., Zhang, X.Y., Liu, Z.J., Ye, H.C., Luo, S.Z., Liu, X.J., Hu, Y., Fang, B., 2017. Spring green-up phenology products derived from MODIS NDVI and EVI: intercomparison, interpretation and validation using National Phenology Network and AmeriFlux observations. Ecol. Indic. 77, 323–336. https://doi.org/10.1016/j.ecolind.2017.02.024.

Piao, S.L., Fang, J.Y., Zhou, L.M., Ciais, P., Zhu, B., 2006. Variations in satellite-derived phenology in China's temperate vegetation. Glob. Change Biol. 12 (4), 672–685. https://doi.org/10.1111/j.1365-2486.2006.01123.x.

Piao, S.L., Liu, Q., Chen, A.P., Janssens, I.A., Fu, Y.S., Dai, J.H., Liu, L.L., Lian, X., Shen, M.G., Zhu, X.L., 2019. Plant phenology and global climate change: current progresses and challenges. Glob. Change Biol. 25 (6), 1922–1940. https://doi.org/10.1111/gcb.14619.

Picornell, A., Buters, J., Rojo, J., Traidl-Hoffmann, C., Damialis, A., Menzel, A., Bergmann, K., Werchan, M., Schmidt-Weber, C., Oteros, J., 2019. Predicting the start, peak and end of the Betula pollen season in Bavaria, Germany. Sci. Total Environ. 690, 1299–1309. https://doi.org/10.1016/j.scitotenv.2019.06.485.

Priyadarshan, P., 2011. Biology of Hevea rubber. Springer.

Richardson, A.D., Andy Black, T., Ciais, P., Delbart, N., Friedl, M.A., Gobron, N., Hollinger, D.Y., Kutsch, W.L., Longdoz, B., Luyssaert, S., 2010. Influence of spring and autumn phenological transitions on forest ecosystem productivity. Philos. Trans. R. Soc. B: Biol. Sci. 365 (1555), 3227–3246. https://doi.org/10.1098/rstb.2010.0102.

Richardson, A.D., Hufkens, K., Milliman, T., Aubrecht, D.M., Chen, M., Gray, J.M., Johnston, M.R., Keenan, T.F., Klosterman, S.T., Kosmala, M., 2018. Tracking vegetation phenology across diverse North American biomes using PhenoCam imagery. Sci. Data. 5 (1), 1–24. https://doi.org/10.1038/sdata.2018.28.

Richardson, A.D., Keenan, T.F., Migliavacca, M., Ryu, Y., Sonnentag, O., Toomey, M., 2013. Climate change, phenology, and phenological control of vegetation feedbacks to the climate system. Agric. For. Meteorol. 169, 156–173. https://doi.org/10.1016/j.agrformet.2012.09.012.

Savitzky, A., Golay, M.J., 1964. Smoothing and differentiation of data by simplified least squares procedures. Anal. Chem. 36 (8), 1627–1639.

Sen, P.K. t, 1968. Estimates of the regression coefficient based on Kendall's tau. J. Am. Stat. Assoc. 63 (324), 1379–1389. https://doi.org/10.2307/2285891.

Shen, M.G., Zhao, W., Jiang, N., Liu, L.C., Cao, R.Y., Yang, W., Zhu, X.L., Wang, C., Chen, X.H., Chen, J., 2024. Challenges in remote sensing of vegetation phenology. Innov. Geosci. 2 (2), 100070. https://doi.org/10.59717/j.xinn-geo.2024.100070.

Shi, C.G., Sun, G., Zhang, H.X., Xiao, B.X., Ze, B., Zhang, N.N., Wu, N., 2014. Effects of warming on chlorophyll degradation and carbohydrate accumulation of alpine herbaceous species during plant senescence on the Tibetan Plateau. PLoS One 9 (9), e107874. https://doi.org/10.1371/journal.pone.0107874.

Takaku, J., Tadono, T., Doutsu, M., et al., 2020. Updates of 'AW3D30'ALOS global digital surface model with other open access datasets. Int. Arch. Photogramm. Remote Sens. Spat. Inf. Sci. 43, 183–189.

Tucker, C.J., 1979. Red and photographic infrared linear combinations for monitoring vegetation. Remote Sens. Environ. 8 (2), 127–150. https://doi.org/10.1016/0034-4257(79)90013-0.

Vermote, E. and Wolfe, R.,2015. MOD09GQ MODIS/Terra Surface Reflectance Daily L2G Global 250 m SIN Grid V006 [dataset]. https://doi.org/10.5067/MODIS/MOD09GQ.006.

Wang, Y.X., Hollingsworth, P.M., Zhai, D.L., West, C.D., Green, J.M., Chen, H.F., Hurni, K., Su, Y.F., Warren-Thomas, E., Xu, J.C., 2023a. High-resolution maps show that rubber causes substantial deforestation. Nature 623 (7986), 340–346. https://doi.org/10.1038/s41586-023-06642-z.

Wang, Q., Moreno-Martínez, Á., Muñoz-Marí, J., Campos-Taberner, M., Camps-Valls, G., 2023c. Estimation of vegetation traits with kernel NDVI. ISPRS J. Photogramm. Remote Sens 195, 408–417. https://doi.org/10.1016/j.isprsjprs.2022.12.019.

Wang, X.Y., Wu, C.Y., Liu, Y.H., Peñuelas, J., Peng, J., 2023b. Earlier leaf senescence dates are constrained by soil moisture. Glob. Change Biol. 29 (6), 1557–1573. https://doi.org/10.1111/gcb.16569.

Waraich, E., Ahmad, R., Halim, A., Aziz, T., 2012. Alleviation of temperature stress by nutrient management in crop plants: a review. J. Soil Sci. Plant Nutr. 12 (2), 221–244. https://doi.org/10.4067/S0718-95162012000200003.

White, M.A., de Beurs, K.M., Didan, K., Inouye, D.W., Richardson, A.D., Jensen, O.P., O'keefe, J., Zhang, G., Nemani, R.R., van Leeuwen, W.J., 2009. Intercomparison, interpretation, and assessment of spring phenology in North America estimated from remote sensing for 1982–2006. Glob. Change Biol. 15 (10), 2335–2359. https://doi.org/10.1111/j.1365-2486.2009.01910.x.

Wolfe, D.W., Schwartz, M.D., Lakso, A.N., Otsuki, Y., Pool, R.M., Shaulis, N.J., 2005. Climate change and shifts in spring phenology of three horticultural woody perennials in northeastern USA. Int. J. Biometeorol. 49, 303–309. https://doi.org/10.1007/s00484-004-0248-9.

Xiao, C.W., Li, P., Feng, Z.M., 2019. Monitoring annual dynamics of mature rubber plantations in Xishuangbanna during 1987-2018 using Landsat time series data: a multiple normalization approach. Int. J. Appl. Earth Obs. Geoinf. 77, 30–41. https://doi.org/10.1016/j.jag.2018.12.006.

Xu, Y.X., Li, X.J., DU, H.Q., Mao, F.J., Zhou, G.M., Huang, Z.H., Fan, W.L., Chen, Q., Ni, C., Guo, K.R., 2023. Improving extraction phenology accuracy using SIF coupled with the vegetation index and mapping the spatiotemporal pattern of bamboo forest phenology. Remote Sens. Environ. 297, 113785. https://doi.org/10.1016/j.rse.2023.113785.

Xu, H. F., Chen, Y. L., Chen, B. Q., R, M. L., Lu, D. S., and Wang, S. S. (manuscript under review). A new framework for mapping rubber plantations through the combination of automatic sample migration, dynamic phenology, and change detection variables based on time series Landsat images.

Yang, X.Q., Blagodatsky, S., Marohn, C., Liu, H.X., Golbon, R., Xu, J.C., Cadisch, G., 2019. Climbing the mountain fast but smart: modelling rubber tree growth and latex yield under climate change. For. Ecol. Manag. 439, 55–69. https://doi.org/10.1016/j.foreco.2019.02.028.

Zeng, L.L., Wardlow, B.D., Xiang, D.X., Hu, S., Li, D.R., 2020. A review of vegetation phenological metrics extraction using time-series, multispectral satellite data. Remote Sens. Environ. 237, 111511. https://doi.org/10.1016/j.rse.2019.111511.

Zhai, D.L., Xu, J.C., 2023. The legacy effects of rubber defoliation period on the refoliation phenology, leaf disease, and latex yield. Plant Divers. 45 (1), 98–103. https://doi.org/10.1016/j.pld.2022.01.003.

Zhai, D.L., Yu, H.Y., Chen, S.C., Ranjitkar, S., Xu, J.C., 2019. Responses of rubber leaf phenology to climatic variations in Southwest China. Int. J. Biometeorol. 63, 607–616. https://doi.org/10.1007/s00484-017-1448-4.

Zhang, X.Y., Friedl, M.A., Schaaf, C.B., Strahler, A.H., Hodges, J.C., Gao, F., Reed, B.C., Huete, A., 2003. Monitoring vegetation phenology using MODIS. Remote Sens. Environ. 84 (3), 471–475. https://doi.org/10.1016/S0034-4257(02)00135-9.

Zhang, J.R., Xiao, J.F., Tong, X.J., Zhang, J.S., Meng, P., Li, J., Liu, P.R., Yu, P.Y., 2022. NIRv and SIF better estimate phenology than NDVI and EVI: effects of spring and autumn phenology on ecosystem production of planted forests. Agric. For. Meteorol. 315, 108819. https://doi.org/10.1016/j.agrformet.2022.108819.

Zhou, R.W., Zhang, Y.P., Song, Q.H., Lin, Y.X., Sha, L.Q., Jin, Y.Q., Liu, Y.T., Fei, X.H., Gao, J.B., He, Y.L., 2019. Relationship between gross primary production and canopy colour indices from digital camera images in a rubber (Hevea brasiliensis) plantation, Southwest China. For. Ecol. Manag. 437, 222–231. https://doi.org/10.1016/j.foreco.2019.01.019.